Resonant Effects of the Violin Tailpiece

Jason Leung

Music Technology Area, Department of Music Research
Schulich School of Music
McGill University
Montreal, Quebec, Canada

December 2015

Abstract

This thesis explores the dynamical relationship between the violin body and tailpiece, with a focus on the effect of tailpiece resonances on the violin's acoustic performance. These resonances are controlled by attaching a series of small masses to several points on the tailpiece, which changes its mass distribution and moment of inertia. To observe the changes in the dynamic behaviour, input admittance measurements were taken at the bridge and several points along the length of the tailpiece. The resulting frequency response functions, when analyzed using a mode-fitting algorithm, demonstrate that a body–tailpiece coupling can occur when the most prominent vibration modes of the body and tailpiece are aligned. This coupling decreases the frequency, quality factor, and magnitude of that body resonance. Informal playing tests reveal that a small mass (around 5 g) is sufficient to audibly temper the brightness of the instrument as well as its wolf note. A similar effect is achieved when a full set of fine tuners is deployed.

Résumé

Cette thèse explore la relation dynamique entre le corps et le cordier d'un violon, en mettant l'accent sur l'effet des résonances du cordier sur la performance acoustique du violon. Ces résonances sont contrôlées par la fixation d'une série de petites masses sur plusieurs points sur le cordier, changeant ainsi sa distribution de masse et son moment d'inertie. Afin d'observer les changements de comportement dynamique, des mesures d'admittance d'entrée ont été prises sur le pont et sur plusieurs points sur la longueur du cordier. Les fonctions de réponse en fréquence obtenues, lorsqu'elles sont analysées en utilisant un algorithme pour le calcul des modes propres de vibration, démontrent qu'un couplage corps–cordier peut se produire lorsque les modes de vibration les plus éminents du corps et du cordier sont alignés. Ce couplage diminue la fréquence, le facteur de qualité, et l'amplitude de la résonance du corps. Les tests informels en situation de jeu révèlent qu'une petite masse (environ 5 g) est suffisante pour tempérer de façon audible la brillance de l'instrument ainsi que sa note de loup. Un effet similaire est atteint lorsqu'un ensemble complet de tendeurs est monté.

Acknowledgments

This work would not have been possible without the support, guidance, and patience of my advisor, Dr. Gary Scavone. His expertise on the subject enabled many new ideas to take root and grow, while his devotion to his students ensured that this project could come to fruition.

I am extremely grateful to my colleagues at the Music Technology Area, and especially to the members of the Computational Acoustics Modeling Laboratory (CAML), who brought many insightful discussions: Connor Kemp, Esteban Maestre, Hossein Mansour, Mark Rau, Charalampos "Harry" Saitis, and Shi Yong. I extend the most sincere thanks to Darryl Cameron and Yves Méthot for their technical assistance during the experiment sessions. And of course, I should never forget my friends (from McGill and beyond) Christopher Antila, Andrew Fogarty, Andrew Hankinson, Andrew Horwitz, Catherine Massie, Alex McLeod, Jordan Miller, Lillio Mok, Lauren Tyros, Gabriel Vigliensoni, Ling-Xiao Yang, and Rosalind Zhang, who provided an abundance of delightful conversations, fond memories, and beer.

Contents

List of Figures

List of Tables

Chapter 1

Introduction

1.1 Motivation

From a scientist's perspective, the acoustics of musical instruments is quite unlike most other topics in science. The *acoustics* part is innocent enough, but the *musical* part, as it were, is far trickier to decipher. What might have been a routine problem in classical physics and materials engineering is suddenly convoluted with aspects of human perception and psychoacoustics. Yet it remains a fascinating topic for many, in large part because music is so prevalent in everyday life. As the noted violin researcher Jim Woodhouse (2014) explains, "…the distinctive flavour of the subject comes from the fact that the key questions are posed by subjective judgments: what is 'good sound'?"

In this regard, the violin is an ideal object to study. Anyone who has attempted to play a violin can attest to the difficulty of drawing out a "good sound" using the bow. But in the hands of a virtuoso, the instrument comes alive, culminating five centuries of refinement at the hands of luthiers. Its high-set floating bridge, arched top and back plates, soundpost, f-holes, and metal-wound strings are just some of the innovations (among many others) that make a violin sound like a violin.

This design has an interesting consequence: the violin's strings cannot be directly attached to the body of the instrument. To maintain the vertical force holding the bridge in place, the strings are lifted off the top plate by the dovetail-shaped tailpiece, which is in turn looped around the end button via the tailgut. Suspended by strings at both ends, the tailpiece acts as a separate resonating mass with its own set of vibratory modes distinct from the instrument body.

The tailpiece inevitably has an influence on the sound of the instrument, but such effects are poorly understood. Even though the majority of scientific investigations of the violin have taken place over the last 50 years, most of those efforts have been directed toward investigating the more prominent components of the instrument: the body, the strings, and the bridge (e.g., Bissinger, 2008). By comparison, the tailpiece has received almost no attention.

At the same time, luthiers are well aware that the tailpiece has some influence on a violin's sound. But as the existing corpus of violin acoustics literature does not address these effects in a systematic way, tailpiece adjustments are typically guided solely by the luthier's experience and intuition, and the optimum solution may be overlooked. The present study will address this dearth of information and provide a scientific perspective on the issues.

1.2 Outline

This work will be presented in the following fashion: First, Chapter 2 will introduce the realm of violin acoustics. Past research on the topic will be presented to form the basis for this work. Chapter 3 will describe the experimental procedure and the data acquisition and analysis tools used. Their advantages and disadvantages will be compared with other techniques commonly used in similar studies. Chapter 4 will present the data collected and propose physical interpretations of the observations. Changes in tone effected by the tailpiece modifications will also be recounted. Finally, Chapter 5 will summarize the conclusions that can be drawn from the results of this study. Implications for luthiers and potential goals for future research will be assessed.

Chapter 2

Background

2.1 The Violin Family

The musical instruments of the violin family are the most popular and recognizable bowed string instruments today. From the immense string choirs of the great symphonies to the intimate settings of small chamber works, the violin, viola, cello (common abbreviation of *violoncello*), and double bass (also *contrabass* or *string bass*) occupy a central role within Western musical traditions. In spite of this, these instruments have remarkably plebeian roots, having been gradually refined by unknown artisans in the remote towns of northern Italy during the early Renaissance. Even though the basic design of the violin and its larger cousins had largely been finalized by the early 16th century, their construction continued to evolve, spurred on by shifting artistic tastes and new innovations and advances in technology (Curtin and Rossing, 2010). By the late 20th century, electric violins have also gained prominence in the popular music scene, even as traditional acoustic violins continue to pervade the popular mindset.

Being bowed string instruments, their primary mechanism for sound production is with a bow, even though players can – and often will – create other musical sounds through other means such as plucking the strings (*pizzicato*), slapping the strings and body, or various other forms of extended techniques. Because of this common trait, many basic facets of the violin also apply to the entire violin family (Curtin and Rossing, 2010). Nonetheless, there are a number of differences in design tailored to the viola, cello, and double bass, usually for ergonomic reasons – in order to be playable, they must be made proportionately smaller compared to the wavelength of the notes within
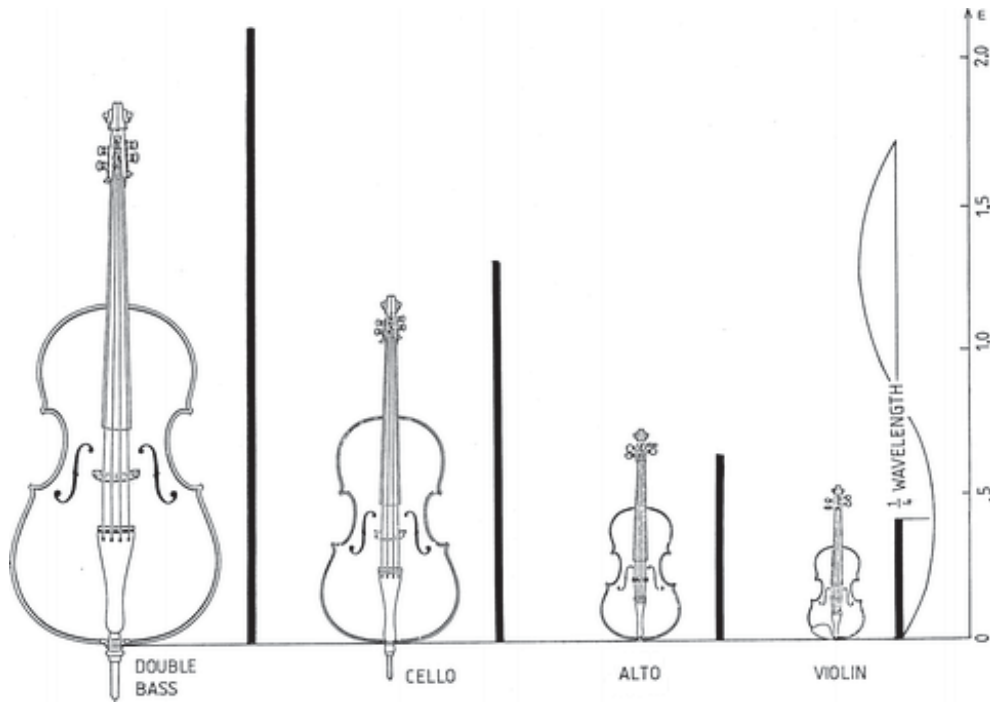
Figure 2.1: The modern violin family compared with the wavelength of the fundamental for their lowest notes. The black bars correspond to one-quarter of the respective wavelengths. "Alto" is an alternative name for the viola. From Askenfelt (2010).

their playing range (see Figure 2.1). In other words, they are not merely scaled-up versions of the violin; each member has its own acoustical signature imparted by its unique structural design (Bynum and Rossing, 2010; Askenfelt, 2010).

2.2 Violin Acoustics

The modern violin is a true marvel of engineering. Each of its components has been meticulously refined by generations of luthiers for a single purpose: the production of music. At first glance, this seems like a regular physics problem, yet this deceptively simple statement has baffled researchers for centuries; how, exactly, does one produce *music*? Only within the past 50 years have researchers truly begun to understand the finer nuances of violin acoustics: Cremer's (1981) monograph *Physik der Geige* (translated into English as *The Physics of the Violin*) is a landmark work in this genre, while extensive surveys of the topic have also been penned by McIntyre and Woodhouse (1978),

Hutchins (1983), and Gough (2000). Most recently, Woodhouse (2014) has contextualized the instrument as only one part of a larger physiological–psychoacoustical system centred on the player – after all, it is the violinist who decides the quality of a violin.

Due to its complexity, the violin is typically broken down into its constituent parts for individual study. An exploded view of the violin is shown in Figure 2.2.

2.2.1 The Strings

Vibrating strings have been used for music throughout all of recorded human history, and, very likely, long before that. Plucked strings, such as harps and lyres, were already known to the ancient Mesopotamians and Greeks, who were masters of elaborate musical systems. In particular, Pythagoras of Samos' work in the 6th century BC relating musical intervals with numerical ratios was monumental in the history of Western music; divisions of the monochord continued to define musical intervals as late as 1722, in Jean-Philippe Rameau's *Traité de l'harmonie* (Nolan, 2002).

By comparison, the bowed string is a much more recent invention. The late development of scraping fibres to against strings for musical purposes likely stems from the fact that it is far easier to make a horrendous noise in this manner than a pleasing sound. Unlike a plucked string, whose vibrations are very well approximated by a linear sum of its natural frequencies, a bowed string is a continuously-driven, self-sustaining nonlinear system characterized by a parameter space largely hostile to "musical" sounds. Whereas a misplayed note on a guitar is still recognizably "musical", a beginning violinist (and those unfortunate enough to be close by) does not have this luxury (Woodhouse, 2014).

At first glance, a bowed string appears to vibrate sinusoidally, much like a standing wave on a freely vibrating string. Over 150 years ago, Helmholtz (1863) demonstrated that a bowed string more closely resembles a triangular shape – two straight portions joined at a sharp bend. This bend races back and forth down the length of the string, reversing its orientation at each end and triggering a transition between the "stick" and "slip" phases of the cycle each time it passes the bow: The string sticks to the bow while the bend travels to the player's finger and back, and slips rapidly across the bow-hair during the shorter trip to the bridge and back (Woodhouse, 2014). Because this happens too quickly for the human eye (hundreds of cycles per second), all that is seen is the curved path outlining the motion of the string. This stick–slip cycle, or "Helmholtz motion", is illustrated in Figure 2.3.
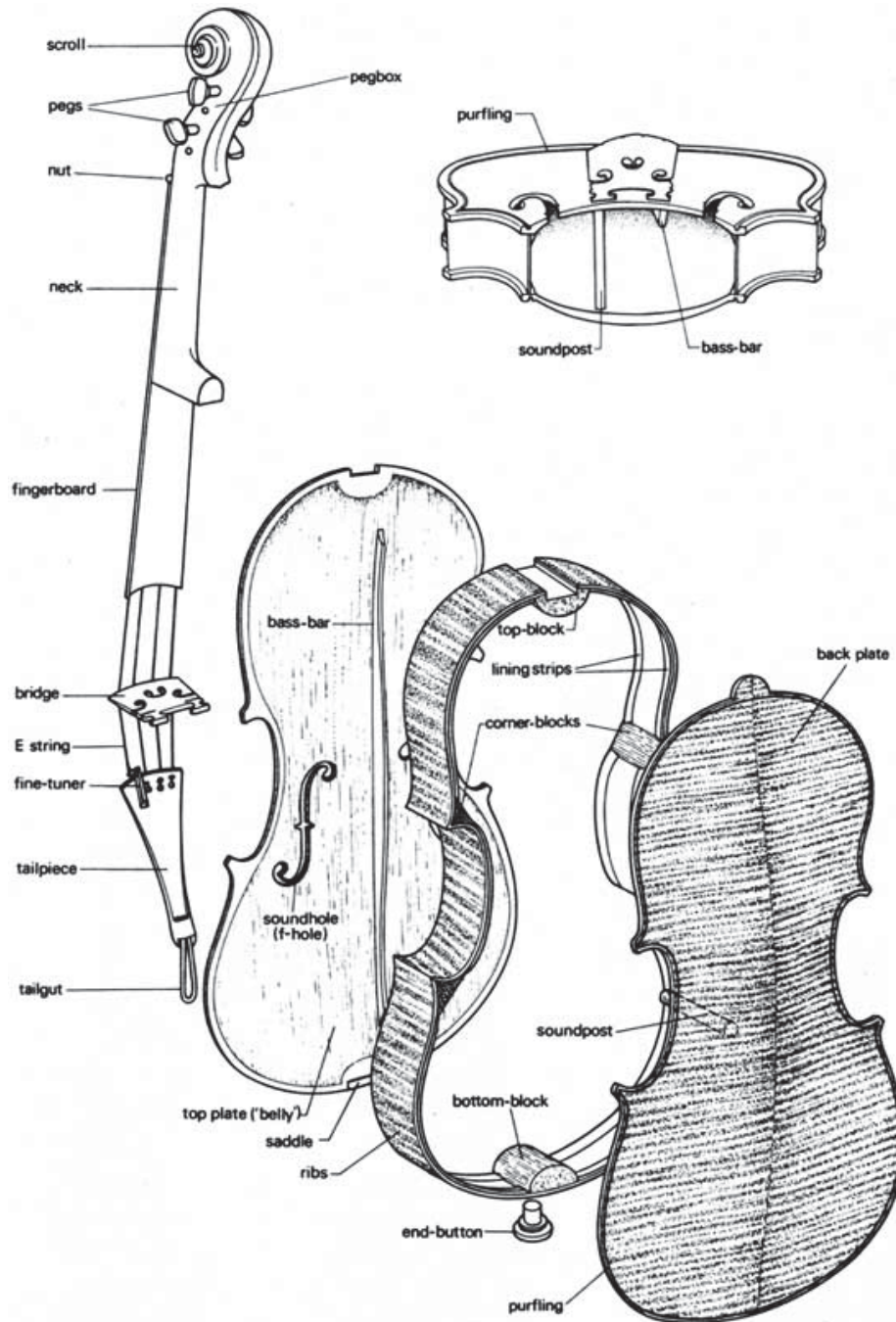
Figure 2.2: An exploded view of the violin. From Johannsson (2015).
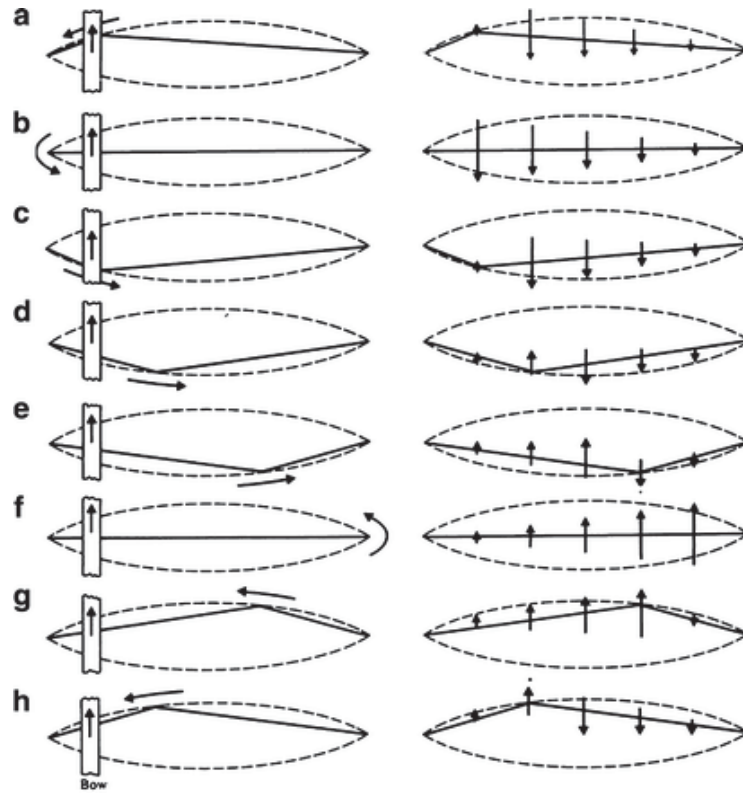
Figure 2.3: A time-lapse representation of Helmholtz motion. (Left) The bend in the string (the "Helmholtz corner") traces out a curved path as it travels along the string; (right) the associated velocities of the string. From Rossing et al. (2002).

As a mechanical waveguide, the string has a characteristic wave impedance, a property that determines its resistance to wave motion along its length or to changes in the wave pattern (Guettler, 2010). Formally, impedance $Z(\omega)$ is defined in the frequency domain as the ratio between force $F(\omega)$ to velocity $V(\omega)$,

$$Z(\omega) = \frac{F(\omega)}{V(\omega)}, \tag{2.1}$$

and is measured in g/s, or mass (displaced) per unit time. On a bowed string, the governing force is the string's tension, T, while the propagating speed is the product of frequency and twice the playing length (one wavelength), $v = 2f\ell$. Alternatively, the wave equation also prescribes a propagating speed of $v = \sqrt{T/\mu}$ on an ideal string, where μ is the density of the string. Combining these observations, the characteristic

wave impedance may be expressed as

$$Z = \frac{T}{2f\ell} = \sqrt{T\mu}. \tag{2.2}$$

In general, the impedance of the string dictates, in the parlance of violinists, its *responsiveness*. When designing strings, manufacturers must carefully balance their physical parameters against musical considerations, a task made more difficult by the lack of known materials with the required tensile strength. Typical values of string density, transverse impedance, tension, and wave propagation speed are provided in Guettler (2010).

2.2.2 The Violin Body

Despite being the defining attribute of the violin family of instruments, the strings, on their own, do not produce or radiate very much sound due to the small amount of air displaced. Instead, their vibrational energy must be transferred to a radiation-efficient wooden (or synthetic) body that can move a much larger volume of air (Gough, 2007; Guettler, 2010). Thus, the body may be characterized as a mechanical amplifier.

However, its frequency response is far from flat. Instead, the body's resonances act as an important filter, adding a distinctive colour that makes a violin sound like a violin (Woodhouse, 2014). Variations in their frequencies, bandwidths, qualities (Q factors), and peak magnitudes govern each instrument's individual character.

For this reason, great emphasis has been placed into uncovering an optimal combination of the resonances. Historically, this has been achieved through centuries of trial and error at the hands of luthiers, but in recent times, technology has greatly aided the task of understanding the violin's structure and design. In particular, the *Strad3D* project (Zygmuntowicz et al., 2009) used CT scans and laser vibrometry to document the geometries and main body resonances of three prized Italian violins: the Titian Stradivari (1715), the Willemotte Stradivari (1734), and the Plowden Guarneri (1735).

Individual components of the instrument have also been isolated and studied to determine their roles in driving the resonances. For example, the bass bar and sound post, besides increasing the overall stiffness of the body, were found to provide an asymmetry vital to exciting several strongly radiating body resonances (Gough, 2013). Meanwhile, the f-holes introduce a monopolar Helmholtz resonance by allowing air to flow in and

out of the instrument (Curtin and Rossing, 2010; Woodhouse, 2014). The f-holes' distinct shape and central placement are thought to have evolved over the centuries to boost the acoustic power efficiency of this mode (Nia et al., 2015).

Nonetheless, caution must be exercised in a strictly reductionist approach. Schleske (1996), for instance, performed experimental modal testing on a violin through each stage of its construction, and found that the boundary conditions changed so drastically that there is no correlation between tuning of the individual plates (Hutchins' (1981) "tap tones") and the resulting frequency spectrum of the violin (up to 1 000 Hz) once it has been assembled.

2.2.3 The Bridge

Unlike the low-set solid bridges found on most string instruments (whether plucked, bowed, or struck), the bridges of the violin family are intricately carved, rest on two feet, lift the strings extremely high off the top plate, and are held in place solely by the tension of the strings (Gough, 2007). This highly unusual design is necessary for translating the mainly lateral vibrations of the string into mainly vertical vibrations of the top plate (Curtin and Rossing, 2010).

The side effects of this innovation are profound. A complicated coupling between the lowest bridge resonance and the "island" – the area on the top plate between the f-holes (Cremer, 1981) – results in a broad peak around 2–3 kHz in the violin's frequency response profile. Named the "bridge hill" by Jansson (1997), this feature is an important ingredient of violin sound, much like a formant in a human vocal tract (Woodhouse, 2014). Further studies on the bridge hill were conducted by Jansson and Niewczyk (1997, 1999), Beldie (2003), and Woodhouse (2005).

2.2.4 The "Wolf Note"

A phenomenon familiar to and yet dreaded by all violinists is the "wolf note", so named because of its characteristic warbling howl-like sound. It occurs at a point where the bridge impedance falls too close to the string impedance, usually due to a strong body resonance; the impedances are said to be matched. When that happens, too much energy is transferred from the string, causing a buildup of vibrational energy at the bridge that interferes catastrophically with Helmholtz motion (Curtin and Rossing, 2010; Guettler,

2010) – the string slips too early in the stick–slip cycle and Helmholtz motion gives way to double slipping motion. Because such motion produces far less energy at the fundamental frequency, the original body vibration is allowed to dissipate. Helmholtz motion is re-established and the cycle repeats, resulting in the distinctive warble (Woodhouse, 2014).

The wolf note most commonly plagues violas and cellos, whose under-sized proportions exacerbate the string–bridge impedance match. On the violin, this effect is most pronounced on the lower strings, which are heavier and thus have a higher impedance. One solution commonly employed by cellists is to attach a metallic mass, called a wolf eliminator, to the string afterlength to dissipate energy from the wolf note resonance. But because wolf eliminators tend to be too bulky for use on a violin or viola, the player's only recourse is to increase the bow force to prevent the double slip from initiating. Unfortunately, doing so also reduces the tonal palette available to the player.

2.2.5 The Tailpiece

The tailpiece is the fixture used to hold the strings. Like all aspects of the violin, its design has evolved over the centuries, but as a highly visible element, it is particularly susceptible to the whims of artistic tastes. Houssay (2014) examined the history of this ornate wooden piece, starting with the cello iconography of the 17th–18th centuries, and through the violin-making treatises of the 19th–20th centuries.

Although luthiers have long been aware of the acoustic influences of the tailpiece, there has been a general lack of interest on this topic. Indeed, Riechers (1895, p.22) remarked that "this part of the instrument exercises a great influence on the tone, although the fact is doubted by a great many performers" – a sentiment that continues to this day. Even as players bicker endlessly over the setup of the strings, bridge, sound post, bass bar, and even the neck and fingerboard, they will routinely settle for an industrially made tailpiece (White, 2012). This was not always so; tool marks on pre-19th-century tailpieces suggest that luthiers had crafted and tuned them to match the instrument to which it was attached. Lamentably, this art has become a casualty of the mass mechanization during the Industrial Revolution (Houssay, 2014).

As a result, no empirical research has been performed on the tailpiece until very recently. Hutchins (1993) first reported enhancements in tone after tuning the tailpiece to the frequency of other violin modes, but it was Stough (1996) who first described
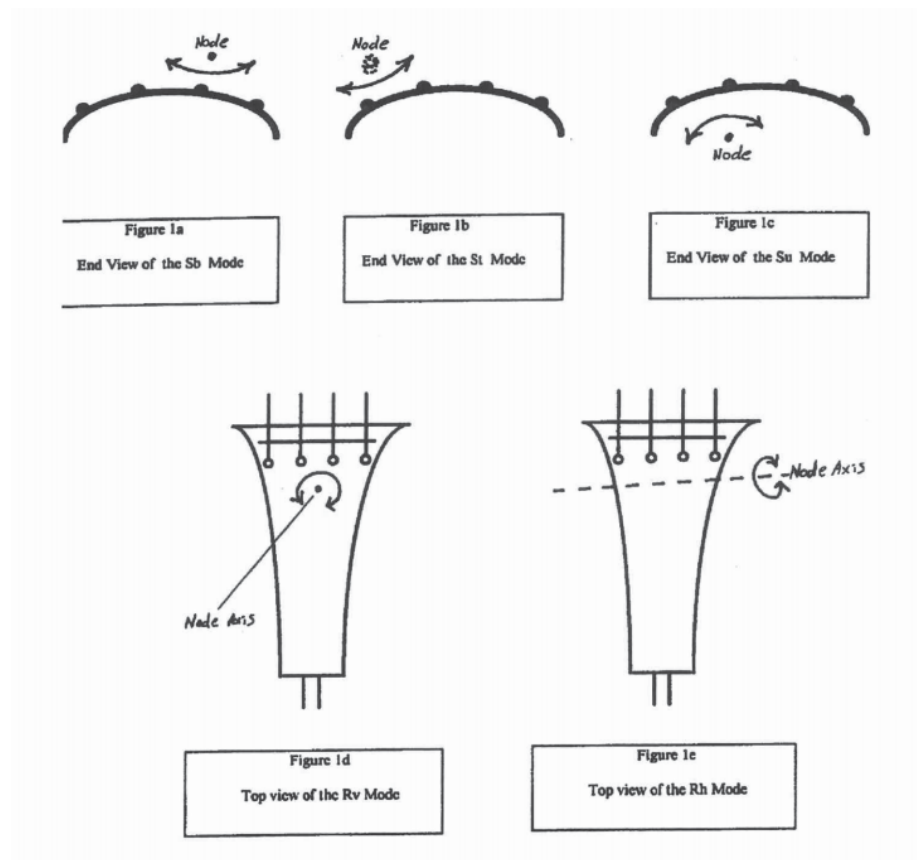
Figure 2.4: Tailpiece modes as depicted by Stough (1996), demonstrating the three "swing" modes (top) and the two rotation modes (bottom).

the vibrational behaviour of the tailpiece itself. He found five of its vibrating modes below 1 500 Hz, where the tailpiece behaved as a rigid body. These modes fell into two classes: three "swing" modes and two rotation modes, as illustrated in Figure 2.4. He also noted that their frequencies depended on the tailpiece mass and tailgut length, and that the two rotation modes could be tuned to modify the main resonance of the violin body. Similarly, Fouilhé et al. (2011) conducted modal analysis on a cello tailpiece and identified nine fundamental modes, seven of which lay well within the natural playing range of the instrument. Experiments in altering the tailpiece mass, as well as its centre of mass, showed significantly different frequency response profiles.

This idea was pursued by White (2012), who recognized the tailpiece's tempering effect on string–bridge vibrations. Collaborating with Pirquet (2011), they developed an adjustable tailpiece with the aim of damping out undesirable resonances. By modifying

the mass distribution of the tailpiece and the length of the tailgut (the looping cord used to attach the tailpiece to the end button), they found that a major tailpiece resonance can be made to couple with the body's wolf resonance, thereby "taming the wolf".

Beyond this, very little is known about the resonant effects of the tailpiece. White suggested that the flexural (torsional) modes may be exploited to alter the timbre of the instrument, as they tend to vary the vertical force applied by the four strings (Fouilhé et al., 2011). However, the method by which this could be done remains unknown.

2.3 Measurements

From a scientific point of view, the primary purpose of a violin is to radiate as much energy as musically tolerable. In this regard, it performs exceptionally well, a feat made even more impressive considering scientific methods were not available throughout most of its illustrious history.

Making observations in a pre-electronic age was extraordinarily troublesome. For instance, the physicist Félix Savart (1791–1841) required constant assistance from the luthier Jean-Baptiste Vuillaume (1798–1875) in assessing various experimental geometries for the violin (Savart, 1819), while Hermann von Helmholtz (1821–1894) had to be content with a vibrating microscope for his bowed string experiments (Helmholtz, 1863). Technology has made great strides in the interim, and the ubiquity of the personal computer has made accurate measurements and complex modal analyses possible even in a luthier's workshop. Because of this, luthiers are now increasingly embracing scientific methods in advancing their craft (Woodhouse, 2014).

2.3.1 Modal Analysis

Modal analysis is a common technique used in structural engineering to study the dynamic response of a structure during excitation, typically by extracting and analyzing modal parameters such as natural frequency, damping factor, modal mass, and mode shape. The structure can either be tested experimentally or modeled on a computer using finite element modeling (FEM) or boundary element modeling (BEM) methods (Curtin and Rossing, 2010). Over the years, every technique developed for structural vibration has been enthusiastically applied to the violin, often as soon as the technology became available (Woodhouse, 2014).

The earliest and simplest electroacoustic measurements involved driving the instrument body with a sinusoidal input, creating operating deflection shapes (ODSs) (Woodhouse, 2014). If the modes are sufficiently far apart, ODSs can reasonably approximate the mode shape, which can be discerned using Chladni patterns. Otherwise, the shape will be the superposition of the overlapped modes and more advanced techniques will be required to separate them. Landmark studies from this era include Backhaus (1930) and Eggers (1959).

The introduction of holographic interferometry in the late 1960s allowed researchers to observe, for the first time, the dynamic behaviour of the violin of the violin body in real time. Ågren and Stetson (1969), Reinicke and Cremer (1970), Jansson et al. (1970), and Jansson (1973) were the earliest adopters of this revolutionary technique.

Since then, holographic methods have largely given way to experimental modal testing, led by advances in computational power and signal processing techniques – especially of the fast Fourier transform (FFT) algorithm. Detailed multidimensional information is first extracted by a set of roving input and output sensors surveying the entire structure. Using Fourier analysis, true mode shapes (rather than ODSs) can be conjured from the resulting transfer functions, as well as their characteristic mass, frequency, and damping parameters. Specialized software can combine these results with finite element methods to build accurate three-dimensional models simulating the dynamic behaviour of the violin (e.g., see Stoppani et al., 2009).

2.3.2 Admittance Measurements

While modal analysis is the most exhaustive method of studying structural dynamics, it requires significant care and time in measuring FRFs at many precisely defined locations on an object, and so it is also the most exhausting method. In practice, the violin is only excited at the string (excluding extended techniques). The resulting vibrations are regulated by the bridge, whose function is twofold: it is both the primary conduit transmitting energy between the string and the body, and the gate reflecting energy back into the string to sustain Helmholtz motion. This observation leads to the notion that the most useful single measure of the acoustical performance of an instrument may be the driving-point impedance at the single point of contact between the string and the bridge (Woodhouse and Langley, 2012).

The driving-point impedance is an important characterization of a structure's dynamic behaviour, as it governs the flow of energy entering and feeding back from the system. Unlike wave impedances, which are properties of individual traveling waves and difficult to isolate in reality, driving-point impedances simply measure the response of a structure to an excitation force and are easily obtained using standard equipment. Ideally, the input and output should correspond to the same spatial point, but since this is physically impossible to measure, careful design is required to obtain accurate results. Finally, Fourier analysis is used to generate frequency response functions (FRFs) of the structure.

The first experiments of this type were independently conducted by the research groups of Cremer and Jansson in the 1970s (Zhang and Woodhouse, 2014). In imitation of a bowing force, the bridge is driven in the bowing direction using an impedance head and strong magnets. Jansson and Niewczyk (1999) later replaced the impedance head with a magnet–accelerometer system attached to the bridge, increasing the range of measurement up to 10 kHz. Since this setup measures the response velocity (converted from the accelerometer) resulting from a driving force, calculations are usually done in terms of the admittance at the bridge rather than the impedance. Admittance $Y(\omega)$ is simply the inverse of impedance (Equation 2.1), relating the driving force $F(\omega)$ to response velocity $V(\omega)$ via the expression

$$Y(\omega) \equiv \frac{1}{Z(\omega)} = \frac{V(\omega)}{F(\omega)}. \tag{2.3}$$

Jansson et al. (1986) experimented with using an instrumented impact hammer rather than a constant magnetic driving force. This lessened the mass-loading effect on the bridge. The process was further refined when Gren et al. (2006) replaced the accelerometer with a laser Doppler vibrometer measurement system. Because impulse hammer measurements are highly portable and easily replicated (they are not dependent on external factors such as room acoustics), they are the most preferred vibration measurement for the study of musical instruments today (Zhang and Woodhouse, 2014).

Hammer measurements are usually conducted only in one direction: To imitate the excitation from a violinist's bow, the hammer strikes against one corner of the bridge in the (idealized) bowing direction of the nearest string, while the accelerometer or vibrometer measures from the opposite corner. In reality, transverse vibrations of the string

occur in two orthogonal polarizations coupled together at the bridge (Woodhouse, 2014), and a player's bowing direction will vary throughout the course of a performance, imposing forces in both directions. Consequently, Lambourg and Chaigne (1993), Boutillon et al. (1988), and Woodhouse and Courtney (2003) acquired multidimensional measurements to depict more completely the vibrational behaviour of the violin. A two-dimensional measurement, for instance, would generate the admittance matrix

$$\mathbf{Y} = \begin{bmatrix} Y_{11} & Y_{12} \\ Y_{21} & Y_{22} \end{bmatrix}, \tag{2.4}$$

where the two subscripts respectively denote the directions of input and output. By convention, the two directions are in the plane of the bridge – the principal plane of vibration caused by the string's transverse vibrations. Measurements are then taken with the hammer and accelerometer (or vibrometer) oriented along each direction. By the principle of reciprocity, admittance matrices are always symmetric (i.e., $Y_{12} = Y_{21}$).

Despite this, a number of luthiers have raised concerns regarding the practice of substituting real bowing gestures with a hammer impact. Zhang and Woodhouse (2014) investigated the reliability and accuracy of the hammer method by carrying out extensive experiments on a cello, comparing three different driving conditions and three different boundary conditions. Their results showed conclusively that "there is nothing fundamentally different about the hammer method, compared to other kinds of excitation."

2.3.3 Microphone Measurements

A study of a musical instrument's acoustic performance cannot be deemed complete without considering the instrument as it is heard by an audience. Supplementing modal analysis and input admittance, microphone measurements can be used to examine the radiation field of a violin. Such experiments can provide answers to the aspects most pertinent to a performance, such as a violin's *carrying power*, or *projection*. As before, researchers can excite the violin using a myriad of techniques depending on the experiment: it could be bowed, struck with an impact hammer, driven with magnetic coils, etc.

The greatest challenge of this kind of experiment, however, comes from the placement of the microphones. Because the violin's radiation pattern is highly dependent on frequency (Meyer, 1972), a single microphone cannot fully capture the entire sound field

of the instrument without being physically moved to different spatial locations. Thus, to obtain the most out of each measurement, researchers usually use multiple microphones. As Curtin and Rossing (2010) recounted, Langhoff (1994) placed five in front of the violin and three behind; Schleske (2002) spaced 36 evenly around the instrument in the plane of the bridge; while Bissinger (2008) arranged 266 in a spherical grid.

2.4 Perception: What makes a "good" violin?

Ultimately, the goal of these measurements is to find relationships between the measurable vibrational properties of instruments and their perceived qualities. This has proved to be a formidable task on both fronts – all attempts to find a scientific criterion describing a "good" violin thus far have been inconclusive.

Even though massive improvements in measurement technologies and analysis techniques have greatly enhanced our understanding of the acoustic behaviour of the violin, Bissinger (2008) found only one "robust" quality differentiator distinguishing the "excellent" violins from the "bad" violins: the Helmholtz resonance was observed to be significantly higher in the excellent violins. All other measures tested revealed no obvious quality-related trends.

Meanwhile, numerous psychoacoustic challenges remain. For example, two violinists will not listen to or judge an instrument in the exact same way, nor would they necessarily use the same verbal descriptions for the same phenomenon. Indeed, investigations by Willgoss and Walker (2007), Fritz et al. (2007, 2010), Saitis et al. (2012), and Wollman (2013) have all found little agreement between listeners – regardless of the demographics of the group – when rating subjective parameters (e.g., liveliness, brightness, responsiveness, etc.). Wollman's study, in particular, stands out since two of the instruments in the experimental pool were actually the same instrument. By outfitting it with an adjustable tailpiece made by White, its centre of mass was shifted between two positions to give the impression of having two different instruments. But despite having similar admittance profiles between the two configurations, listeners assigned ratings that were, on average, as diverse as those between two physically distinct instruments. This suggests that violinists are extremely sensitive to slight differences in the admittance curve, but precisely how these differences might affect their perceptual judgments of the instrument is not currently known.

Chapter 3

Experiment Procedure

The main purpose of this study is to explore the effect of tailpiece resonances on the violin's acoustic performance. Stough (1996) and White (2012) showed that a small mass placed strategically on the tailpiece can be used to dampen the violin's main body resonance, but beyond this, little is known about the dynamical relationship between the violin body and the tailpiece. This study will build upon their work in a systematic way, as well as attempt to address the physical mechanism behind the body–tailpiece coupling.

3.1 Equipment

The violin used in this experiment was made in 2005 by H. Armenious, a luthier operating in Toronto, Canada. It was chosen because of its expert craftsmanship, ensuring that its properties can be readily compared with other violins. The violin was equipped with a set of Thomastik–Infeld Peter Infeld strings held under standard tension (Table 3.1), aurally tuned in just intonation with the A4 set to 440 Hz. A Hill model fine tuner fastens the E-string onto a Hill model tailpiece, which is 113 mm long and constructed of rosewood. After tuning, the afterlength measures 52 mm from the bridge to the "fret" on the tailpiece, while the tailgut extends 39 mm from the tailpiece (78 mm around the whole loop). All non-essential accessories, including the chin rest, were removed so that the body could vibrate as freely as possible.

The input force was generated by a Piezotronics miniature instrumented impact hammer (model 086E80), whose 2.5 mm-diameter conical tip can precisely strike the thin edges of the bridge. Two tips were supplied by the manufacturer, a stainless steel

String	Core	Winding	End	Tension (kg)
E	Chrome steel	Platinum plated	Ball	8.3
A	Synthetic	Aluminum	Ball	5.5
D	Synthetic	Silver	Ball	4.8
G	Synthetic	Silver	Ball	4.7

Table 3.1: Properties of the strings equipped on the violin, provided by the manufacturer.

tip (hard) and a vinyl impact cap (soft). Despite the stainless steel tip's tendency to leave indentations on the wooden bridge, it was preferred over the vinyl cap because the cap reduced the frequency response of the impact to as low as 1 kHz, severely disrupting a significant portion of the signal.

A Polytec portable laser vibrometer (PDV100) recorded the vibration velocities. Choosing a laser Doppler vibrometer over an accelerometer is advantageous for two reasons: First, there is no added mass that can modify the vibration response of the instrument; Zhang and Woodhouse (2014) demonstrated that even a lightweight (0.3 g) accelerometer can have profound effects upon a violin's bridge admittance measurements – including the complete elimination of the bridge hill. Second, the laser can be pointed at any location and in any direction without moving the instrument. However, the main drawback is that the instrument must be held absolutely stationary.

The signal from the hammer was amplified tenfold by a Piezotronics line-powered signal conditioner (model 482C16). Finally, a National Instruments analog data acquisition board (NI USB–4431) collected the amplified force and vibration signals and transferred them to a PC for processing in MATLAB.

3.2 Experiment Setup

Measurements were taken in two rooms at McGill University, first at the Spatial Audio Laboratory (located within the Centre for Interdisciplinary Research in Music Media and Technology), and then at the Computational Acoustic Modeling Laboratory. The change in environment – implemented purely for logistical reasons – was not anticipated to cause drastic changes to the experiment; room acoustics play a negligible role in input admittance measurements (Zhang and Woodhouse, 2014). See §3.5 for further discussion of this topic.

In order to approximate "free–free" boundary conditions, the violin was vertically suspended from a rigid fixture on the ceiling (in both rooms) using a string looped around the scroll. Soft foam was placed lightly under the end button, partly to support the instrument, and partly to subdue the induced low-frequency "swinging" caused by the hammer's impact. Sufficient manœuvrability around the point of contact was maintained to ensure that only this low-frequency contamination (which lies below the range of interest for these measurements) is damped. Other than these boundary conditions, no other point on the instrument body was in contact with an external object. A piece of cardboard and two small pieces of foam were strategically placed along the playing length of the strings to prevent their resonances from interfering with those of the body, but these dampeners were not in contact with the violin body. Figure 3.1 shows the setup in the Spatial Audio Laboratory, which was replicated as closely as possible when the experiment moved to the Computational Acoustic Modeling Laboratory.

The impact hammer was secured onto a vertically adjustable altitude–azimuth mount. Like a pendulum, it swings freely along the altitude axis to ensure that impacts would consistently land at the same position with roughly the same force. Nonetheless, filling in the two-dimensional admittance matrix (Equation 2.4) required the instrument to be struck and measured along both directions. And with only one laser available, the (symmetric) cross-terms must be measured separately from the on-axis terms. Thus, the hammer and laser had to be moved manually to obtain the three measurements (two on-axis terms and one cross-axis term). The hammer and laser each had its own stand so that their movements would not affect the free-swinging violin.

3.3 Data Acquisition

As in previous studies of this kind (e.g., Bissinger, 2008), the impact hammer was positioned to strike on the bass (G-string) side of the instrument. Ideally, the point of measurement should coincide with the strike. But since this is physically impossible, the laser beam is aimed at the closest possible point instead. The need to take two-dimensional measurements further restricted the selection of impact points to areas lying along edges where perpendicular surfaces met – the laser cannot be pointed at a location within the interior of the wood. Consequently, the upper bass-side corner was designated as the impact point on the bridge (Figure 3.2a), while four points were selected along the same side on the tailpiece (Figure 3.2b and Table 3.2).

Figure 3.1: The experiment setup in the Spatial Audio Laboratory. From left to right are: the laser vibrometer, the hammer and pendulum secured on an altazimuth mount, and the violin suspended from the ceiling and gently supported by foam.
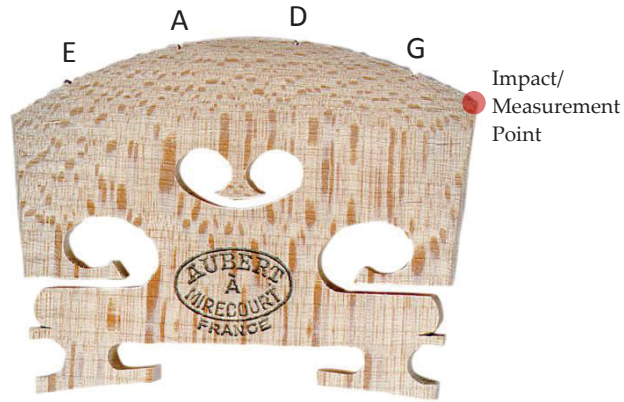
(a) Bridge
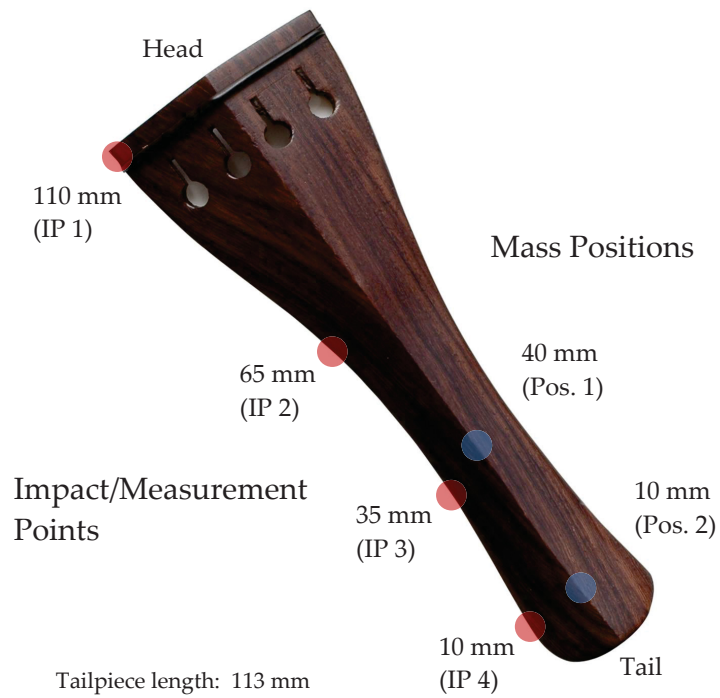
(b) Tailpiece

Figure 3.2: Selected points for measurement (red circles) and placement of masses on the tailpiece (blue circles).

Impact/measurement point	Distance from tail end (mm)
IP 1	110
IP 2	65
IP 3	35
IP 4	10

Table 3.2: Selected points on the tailpiece for measurement, all located along the bass (G-string) side edge. Distances are measured along the central (lengthwise) axis. The tailpiece is 113 mm long.

The first set of experiments involved attaching small metal masses to the tailpiece. Including the putty used to fasten them, their total masses were 2.5, 5.5, and 16.0 g ($\pm$0.25 g). In turn, they were placed 40 mm and 10 mm from the tail end, along the central axis (Figure 3.2b). The second set of experiments compared the use of one versus four fine tuners. Hill model fine tuners, preferred for their small size, were used; each weighed 5.0 ± 0.25 g.

Prior to each set, reference measurements were taken with no masses attached to the instrument (except the E-string fine tuner) in order to evaluate the change incurred by the subsequently added mass. For each configuration, input admittance measurements were taken at the five selected points (one on the bridge and four on the tailpiece).

Each impact was recorded for 2 s at a sampling rate of 44 100 Hz. To ensure consistent recordings, an auto-triggering mechanism listened for an impact event (> 0.09 N) and began recording from four samples before the impulse peak. To increase the signal-to-noise ratio, five impact events were recorded and averaged to form a single measurement. Three measurements – two on-axis and one cross-axis – were collected for each selected point.

3.4 Data Analysis

All data collection and analysis was conducted using the MATLAB program *DAQPlot* developed by G. Scavone and J. Woodhouse (personal communication, 2015). For each impact event, a frequency response function (FRF) was immediately calculated and averaged among previously recorded events (if any). Phase delays attributed to the measurement equipment were also digitally corrected at this point.

During the averaging, a coherence function was also calculated as a measure of the linearity of the measurement – a coherence of unity throughout the frequency spectrum is considered ideal. Thus, the coherence could be used to evaluate an impact event's quality, as faulty strikes occasionally occur, resulting in drastically different FRFs. Without having to inspect the FRFs from the other impact events (which may be difficult), the coherence function provided the information at a glance. Such faulty impact events were unceremoniously discarded.

3.4.1 Mode Fitting

A two-dimensional mode fitting algorithm developed by Maestre et al. (2013) was used to identify the resonant modes in the spectra. It employed spectral peak processing to estimate and optimize mode natural frequencies and bandwidths from input admittance measurement data.

In this scheme, the violin was first assumed to be a linear system, meaning that the whole system could be broken down into the sum of individual resonant elements (modes). As in Bank and Karjalainen (2010), a set of structurally passive (i.e., positive-real) D-dimensional admittance matrices was expressed in the digital domain as

$$\hat{\mathbf{Y}}(z) = \sum_{m=1}^{M} H_m(z)\,\mathbf{R}_m, \tag{3.1}$$

where the gain $\mathbf{R}_m$ is a $D \times D$ positive-semidefinite matrix, and each mode

$$H_m(z) = \frac{1 - z^{-2}}{\left(1 - p_m z^{-1}\right)\left(1 - p_m^* z^{-1}\right)} \tag{3.2}$$

is a second-order resonator determined by the complex conjugate poles p_m and p_m^*.

From this, Maestre et al. (2013) presented an error minimization problem $\varepsilon(\mathbf{Y}, \hat{\mathbf{Y}})$ between the admittance matrix $\mathbf{Y}$ and the admittance model $\hat{\mathbf{Y}}$, subject to the constraint that $\mathbf{R}_m$ must be positive-semidefinite. The error was minimized iteratively, with the kth iteration defined as

$$\varepsilon\left(Y, \hat{Y}\Big|_k\right) = \sum_{n=1}^{N} \left| \log \frac{|Y_n|}{\left|\hat{Y}_n\right|_k} \right| \tag{3.3}$$

for N-sample long vectors $Y(\omega)$ and $\hat{Y}(\omega)$ taken in $0 \leq \omega < \pi$. When expressed in a logarithmic scale, Equation 3.3 reduces to a difference of magnitudes.

Finally, the MATLAB software package *CVX* (Grant and Boyd, 2008, 2014) conducted convex minimization to find a set of parameters H and $\mathbf{R}$ such that $\varepsilon(\mathbf{Y}, \hat{\mathbf{Y}})$ was minimized within a selected frequency range. In this study, optimization was performed between 100 and 6 000 Hz, where measurement coherence was closest to unity.

3.5 Repeatability of Measurements

Although utmost care was taken to ensure the experiment conditions remain identical across all measurements, variations between measurements will inevitably arise due to the nature of this experiment. For example, incremental disruptions from the hammer strikes not only have a propensity to move the instrument, but they also leave indentations – albeit small – on the wooden impact surfaces, making each impact slightly different from the last. But while such minor variations were, by and large, eliminated by the averaging process, other factors cannot be so controlled.

Zhang and Woodhouse (2014) tested the repeatability of such experiments by making identical measurements ten months apart. While the two admittance measurements exhibited general agreement, there were noticeable deviations – up to 5 dB and 5 Hz – in individual modal amplitudes and frequencies ascribable as the margin of error of the experimental procedure. Thus, even though room acoustics are not a significant factor in this sort of experiment, there can be other factors at play.

In particular, the experiment here involved constant changes in setup. To wit, the hammer and laser's frequent relocations (to obtain data from different directions) induce mechanical vibrations in the floor that could, in theory, affect the violin's supporting mount. But more importantly, the two sessions of the experiment occurred in different rooms and different seasons (late winter vs. early summer). Environmental influences, such as air temperature and humidity, could significantly alter the wooden instrument's structure. Although the two laboratories are both climate controlled, the extent to which the violin was affected is difficult to ascertain. With this in mind, comparisons should only be drawn between measurements taken during the same session.

Chapter 4

Results

The results of attaching various masses to the violin tailpiece are presented in this chapter. Measurements of a violin's input admittance can offer significant insight into the violin's vibrational properties (Woodhouse and Langley, 2012). Because the bridge is excited by two orthogonal polarizations for a string's transverse vibrations, a two-dimensional driving-point admittance matrix is gathered to gain a more complete picture of this behaviour (Equation 2.4). Measurements were taken with the impact hammer and laser Doppler vibrometer oriented parallel and perpendicular to each other, but since the 2×2 admittance matrix $\mathbf{Y}(\omega)$ is assumed to be symmetric (i.e., $Y_{12} = Y_{21}$), the system can be completely described with only three measurements rather than four. In this text, direction 1 points parallel to the top plate (from the G-string toward the E-string) while direction 2 is perpendicular to the top plate (from the top plate outward), as shown in Figure 4.1.
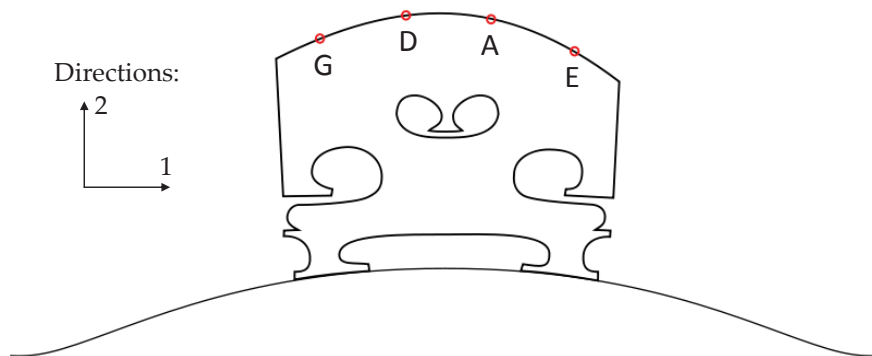
Figure 4.1: The measurement directions.

4.1 Reference Measurements (unmodified violin)

Reference measurements were taken with the violin unmodified (i.e., with no mass attached) prior to every data collecting session. As discussed in Section 3.5, variations inevitably arise regardless of the steps taken to ensure consistency. This was further exacerbated by the fact that the data was collected over multiple sessions, where the setup was torn down and rebuilt each time. Establishing a ground truth for each set is therefore crucial to making comparisons across data sets: Even though absolute changes across data sets cannot be directly compared, relative changes – i.e., deviations from the respective reference measurements – can be.

4.1.1 Frequency Response: Bridge

Two-dimensional frequency response functions (FRFs) taken at the violin's bridge are shown in Figures 4.2 and 4.3. Typical features of a violin's response profile can be readily seen: prominent peaks that dominate the FRFs up to roughly 1 kHz (the "signature modes") and a single broad, yet densely populated peak between 2 and 3 kHz (the "bridge hill").

Individual FRF measurements provide no information about mode shapes. Thus, resonances found in FRFs cannot be uniquely identified with specific signature modes without performing modal analysis. That said, the signature modes routinely fall in particular frequency ranges because all violins have similar geometries (Stoppani et al., 2009; Gough, 2013). Henceforth, observed peaks in the FRF results will be associated with specific signature mode names based on their expected frequency ranges.

Mode	Full name	Frequency (Hz)	Q
A0	Fundamental air resonance	283	33.5
CBR	Centre bout romboid	416	50.3
A1	Second air resonance	470	54.0
B1−	First "breathing" mode	494	50.5
B1+	Second "breathing" mode	588	38.4

Table 4.1: Resonances observed in the bridge FRF (Figure 4.2) postulated to be those described by Stoppani et al. (2009). Values listed are the average between the two measurement sessions.

Mode	Full name	Frequency (Hz)	Q
Sb	Swing mode, bass side	100–140	50–80
St	Swing mode, treble side	120–160	60–90
Su	Swing mode, under	180–230	35–70
Rh	Rotation, horizontal axis	300–800	34–110
Rv	Rotation, vertical axis	300–800	38–110

Table 4.2: Tailpiece resonances identified by Stough (1996). The frequencies and Qs are given by ranges since their precise values depend on the tailpiece's setup.

Several resonances are also spotted in the spectrum around 135, 210, and 650 Hz. As it turns out, these are tailpiece resonances, a direct consequence of leaving the afterlength undamped. These modes will be discussed in the next section (§4.1.2).

Besides the signature modes, bridge hill, and tailpiece resonances, there are no other significant features to be discerned. Below 100 Hz, the violin does not have any significant resonances, and the spectrum is instead dominated by the resonances of the support rig. Above 10 kHz, the signal becomes concealed by noise due to insufficient impact (input) energy.

4.1.2 Frequency Response: Tailpiece

Hammer measurements taken on the tailpiece reveal the vibrational behaviour of the system from the tailpiece's point of view. Unlike the bridge, measurements were taken at multiple points on the tailpiece (Figure 3.2b); the collected FRFs are presented in Figures 4.4 and 4.5.

The observed tailpiece resonances can be matched with those in Stough (1996). As can be seen by comparing Tables 4.2 and 4.3, there is very good agreement between the values found by Stough and by this experiment. But as with the signature modes of the violin body, modal analysis is required to verify their identities, and the matching of the observed modes to those identified by Stough is purely conjectural.

All of the modes identified in Table 4.3 are rigid-body modes; this is attested by noting that their values are uniform along the length of the tailpiece. Also, all of these rigid-body modes quite conveniently lie in the region of interest between 100 and 1 000 Hz. If Fouilhé et al.'s (2011) work on the cello tailpiece carries over to the violin tailpiece, then these are the only rigid-body modes of the tailpiece – all higher-frequency resonances are torsional.
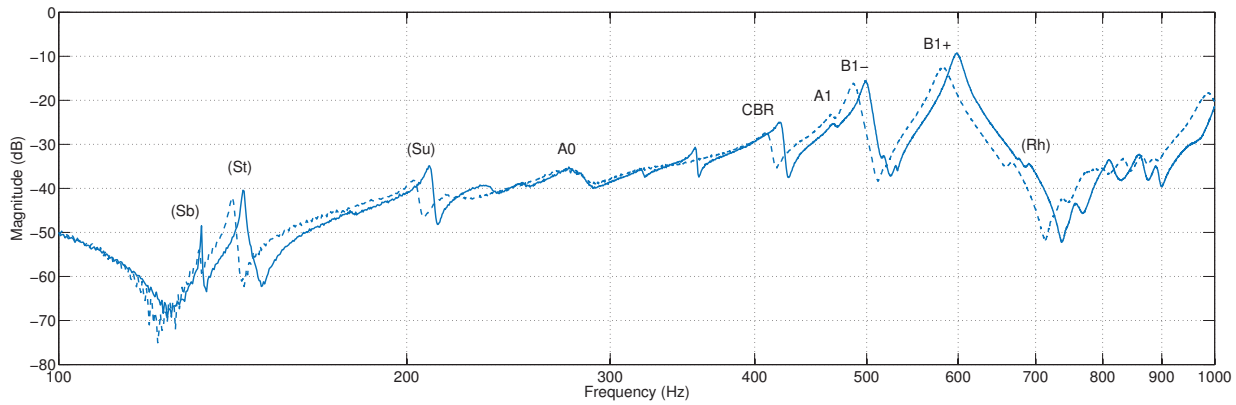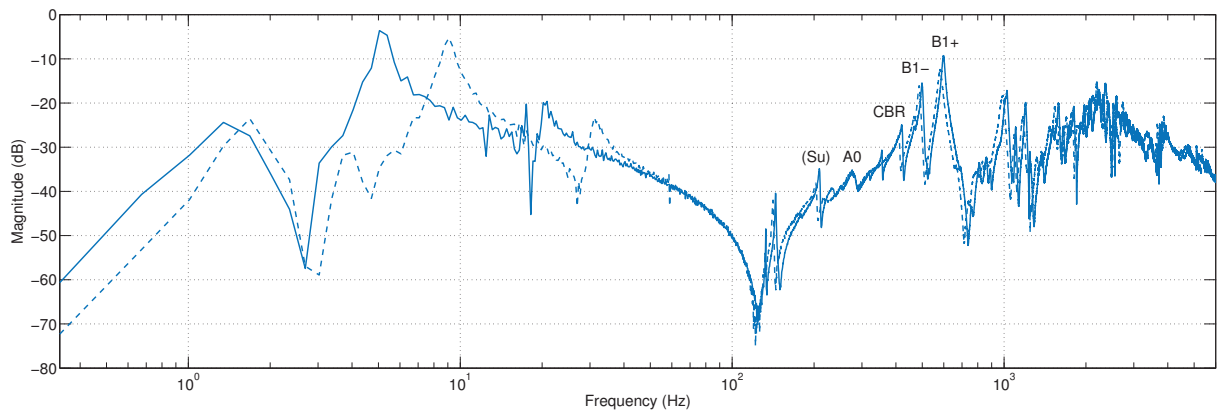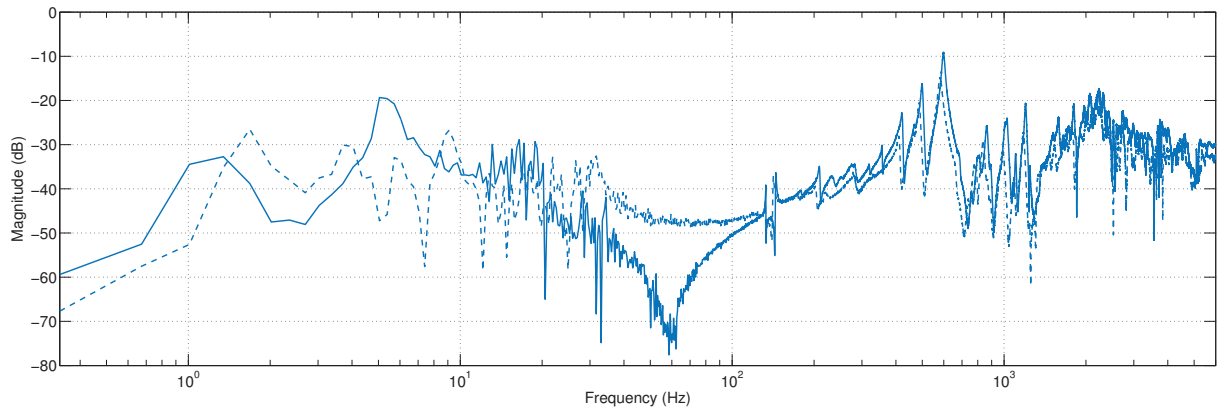
(a) (1,1)–direction
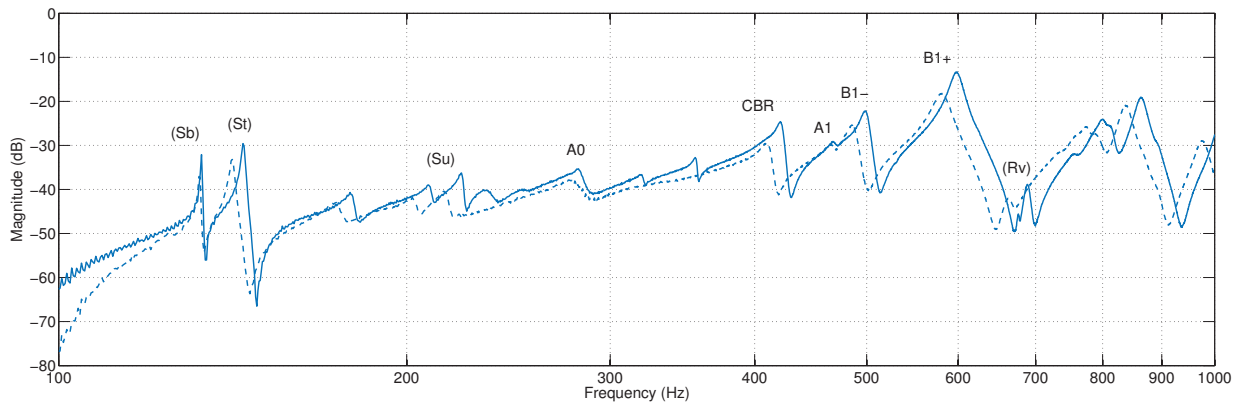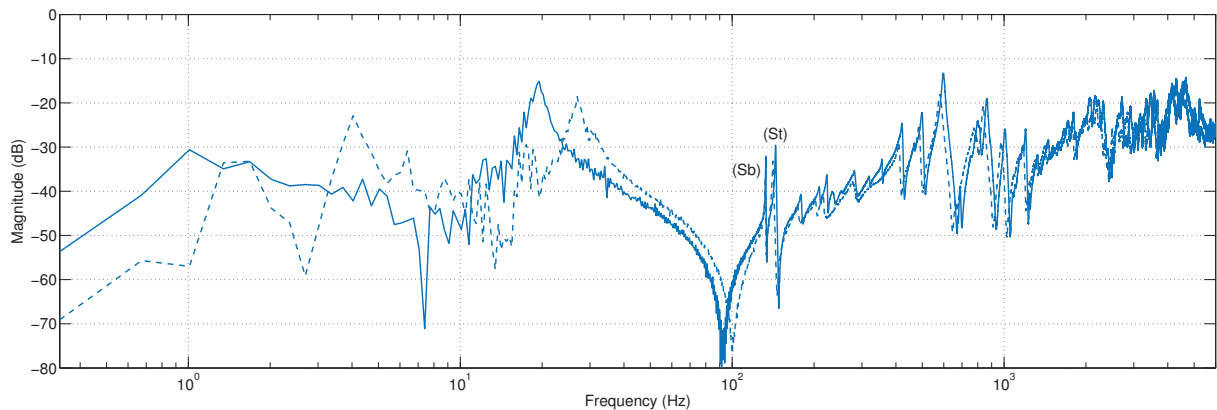

(b) (2,2)–direction

Figure 4.2: FRFs for two selected directions (top and bottom) taken from the bridge of an unmodified violin. The direction tuples refer to the directions of excitation and measurement respectively. The solid and dashed lines refer to the two measurement sessions. Labeled are the body resonances postulated to be those described by Stoppani et al. (2009); in parentheses are tailpiece resonances most likely to be those in Stough (1996). FRFs over a greater frequency range are shown in Figure 4.3.

(a) (1,1)–direction
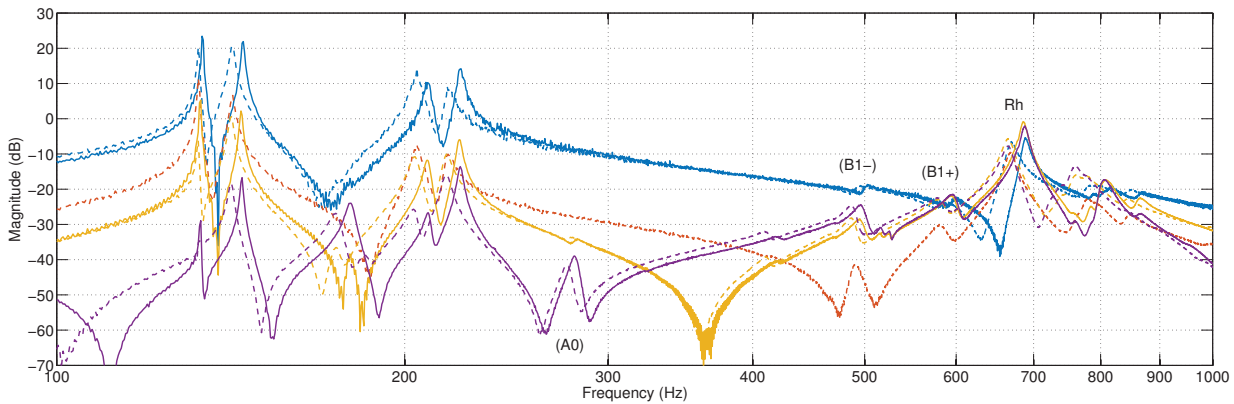

(b) (1,2)–direction

(c) (2,2)–direction

Figure 4.3: Bridge FRFs of an unmodified violin. The direction tuples refer to the directions of excitation and measurement respectively. The solid and dashed lines refer to the two measurement sessions. Labeled are the body resonances postulated to be those described by Stoppani et al. (2009); in parentheses are tailpiece resonances most likely to be those in Stough (1996).
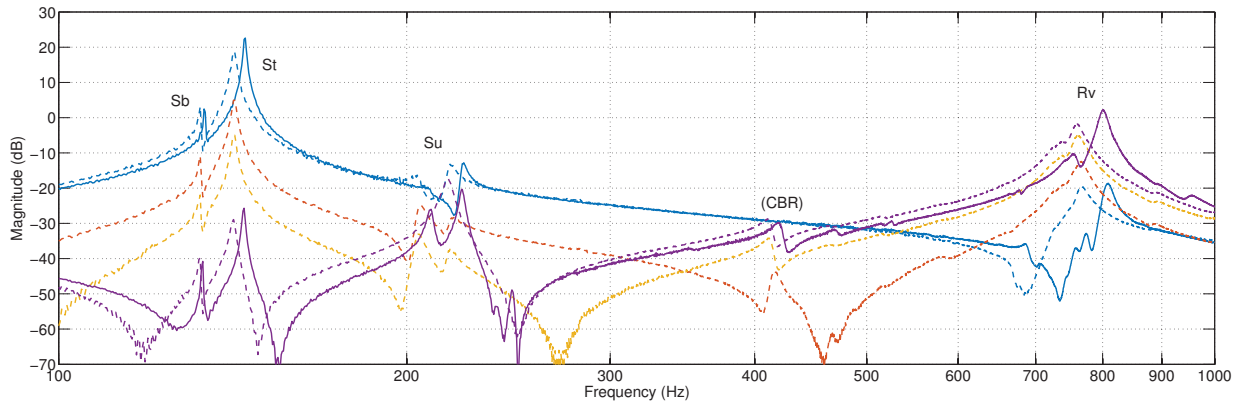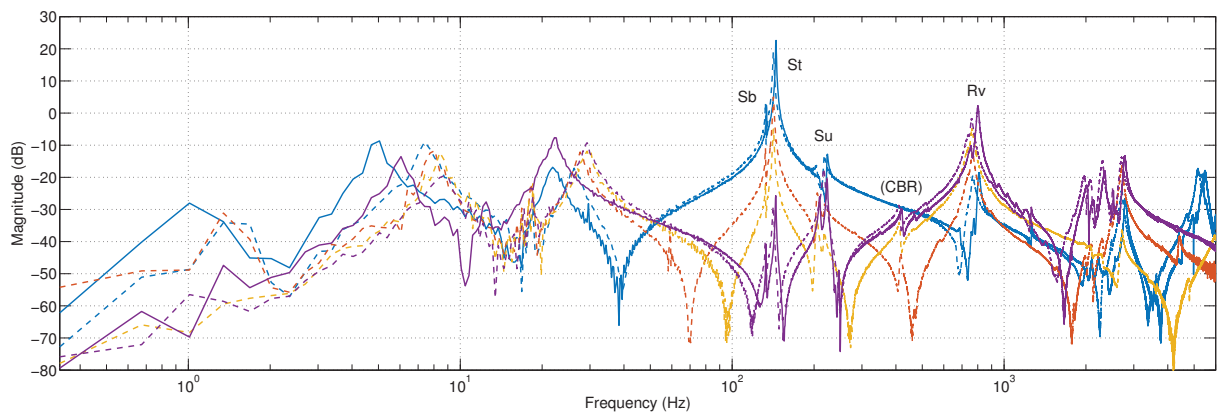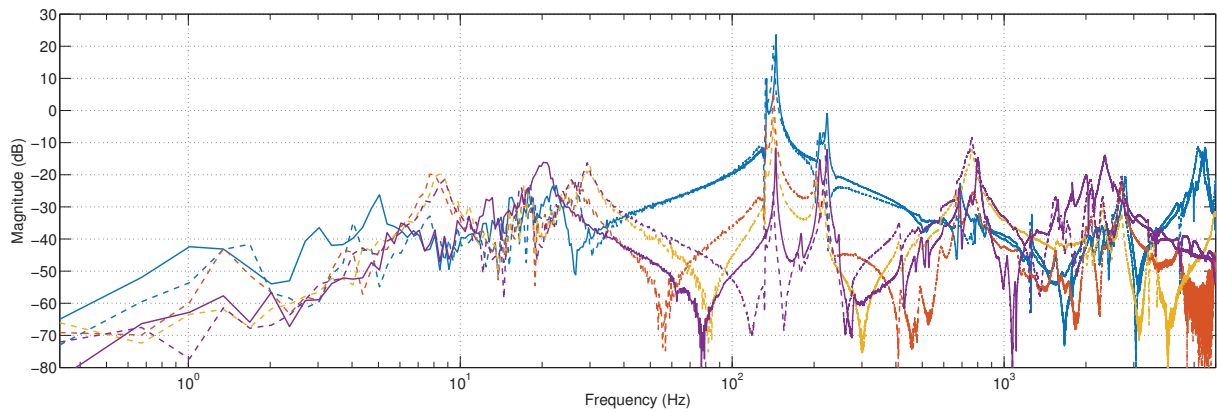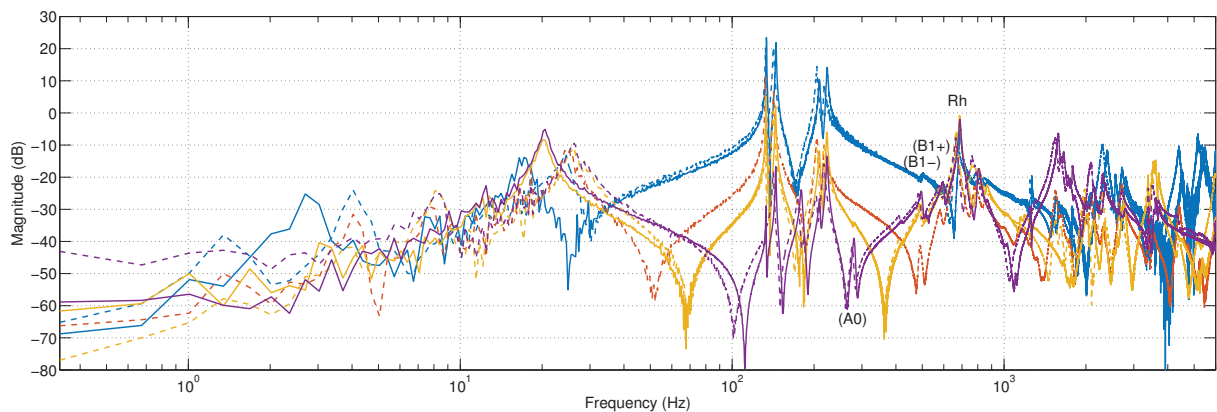
(a) (1,1)–direction

(b) (2,2)–direction

Figure 4.4: Tailpiece FRFs for two selected directions (top and bottom) taken at four points along the tailpiece. The colours blue, red, gold, and purple refer to the four impact/measurement points (IP 1–4 respectively), while the solid and dashed lines refer to the two measurement sessions. Labeled are the tailpiece resonances most likely to be those identified by Stough (1996); in parentheses are body resonances postulated to be those described by Stoppani et al. (2009). FRFs over a greater frequency range are shown in Figure 4.5.

(a) (1,1)–direction

(b) (1,2)–direction

(c) (2,2)–direction

Figure 4.5: Tailpiece FRFs taken at four points along the tailpiece. The colours blue, red, gold, and purple refer to the four impact/measurement points (IP 1–4 respectively), while the solid and dashed lines refer to the two measurement sessions. Labeled are the tailpiece resonances most likely to be those identified by Stough (1996); in parentheses are body resonances postulated to be those described by Stoppani et al. (2009).

Mode	Frequency (Hz)				Q			
Sb	133	133	133	133	73.6	69.6	73.3	94.8
St	142	142	143	142	59.1	64.7	59.5	52.0
*Su	205	205	205	205	50.0	58.6	56.9	81.2
	218	218	218	217	72.5	48.5	49.5	79.7
Rh	667	668	666	666	38.7	38.7	38.9	38.1
Rv	761	763	759	758	26.0	30.9	26.6	32.6

Table 4.3: Tailpiece resonances identified from Figure 4.4. In each category, the four columns represent the four impact/measurement points (IP 1–4 respectively). Values listed are the average between the two measurement sessions. *Su is a split peak.

In the portrait gathered in Figures 4.4 and 4.5, the swing modes and rotation modes are seen to influence the tailpiece non-uniformly: Near the head of the tailpiece (closest to the bridge), the swing modes dominate; whereas near the tail end, the rotation modes prevail. However, Stough has observed that the three swing modes have little effect on the violin's tonal output. This is perhaps unsurprising, as they all lie well below the signature modes of the violin. The rotation modes, by contrast, lie just above them.

But surveying the tailpiece plots reveals a peculiar feature: the presence of the body modes within the tailpiece signal, especially near the tail end (compare the blue (IP 1) and purple (IP 4) curves of Figure 4.4). In itself, this is not particularly surprising since the tailpiece is fixed to the top plate via the tailgut. Tautly stretched, the tailgut couples the two components together quite effectively, allowing them to vibrate in tandem. Near the saddle (where the tailgut bends around the top plate), the CBR mode is torsional roughly about the central (lengthwise) axis, yet moving chiefly in direction 1, while the two breathing modes pulsate in direction 2 (Stoppani et al., 2009; Gough, 2013).

Thus, the path forward is clear: attempt to couple the rotation modes with the violin's breathing modes. The simplest method to lower the frequency of a resonance is to add mass to the region of greatest amplitude (an antinode). In this case, that would be toward the tail end of the tailpiece.

4.2 Mass-loaded Tailpiece

There are two independent variables in this experiment: the mass and its position. In succession, three small masses (2.5, 5.5, and 16.0 g) are placed at two positions on the

Mode	Frequency (Hz)			Q			Direction 1 magnitude (dB)			Direction 2 magnitude (dB)		
A0	284	283	283	43.0	27.0	40.4	−40.7	− 46.7	− 40.4	−39.4	− 43.8	− 43.3
CBR	421	420	420	56.9	57.5	57.5	−25.0	− 28.1	− 24.1	−24.1	− 28.4	− 29.0
A1	471	471	471	55.4	45.7	38.6	−45.4	− 48.3	− 37.3	−45.3	− 47.7	− 48.1
B1−	500	498	495	50.0	45.7	40.1	−15.3	− 19.5	− 19.0	−20.1	− 29.6	− 33.5
B1+	596	590	588	43.2	31.4	25.2	−12.7	− 15.6	− 15.9	−15.8	− 21.0	− 25.0

Table 4.4: Effect of a 2.5 g mass on the signature modes. In each category, the three columns represent the measured values (from left to right) with the mass off, and with it attached at positions 1 and 2.

tailpiece (40 mm and 10 mm from the tail end; Figure 3.2b) to study the effects on the bridge and tailpiece FRFs.

4.2.1 2.5-gram mass

The lightest mass attached was 2.5 ± 0.25 g. The resulting bridge FRFs are shown in Figure 4.6, while the values of the signature modes are given in Table 4.4. Notably, the properties of the two breathing (B1− and B1+) modes display a clear correlation with the position of the mass – placing the mass closer to the tail end is accompanied by a reduction in both frequency and amplitude, as well as a broadening, of the peaks. This suggests that the tailpiece plays a non-negligible role in shaping the bridge FRF and, consequently, the vibrational characteristics of the violin. To explore the mechanism behind this coupling, the tailpiece FRF, as measured at four locations, is presented in Figure 4.7.

All of the tailpiece modes identified in Table 4.3 were noticeably affected. But with a lack of prominent body resonances near the three swing modes, the following analysis will focus exclusively on the two rotation modes.

Like the signature modes, the rotation modes responded to the added mass with a reduction in frequency and magnitude, only much more dramatically – the Rv mode (as measured at IP 1) shifted from 806 to 721 Hz and dropped from −22.0 to −37.5 dB, while the Rh mode shifted from 692 to 635 Hz and fell from −10.0 to −17.5 dB. Given that the tailpiece is much less massive than the violin body, this was not unexpected.
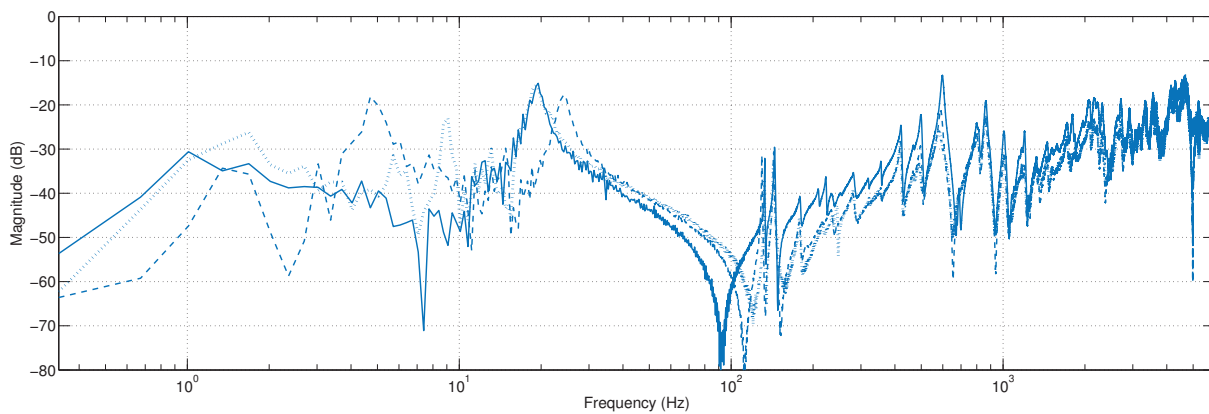
What is most fascinating though, is that lowering the Rh mode's frequency causes some of its energy to be transferred to the B1-induced modes on the tailpiece (compare
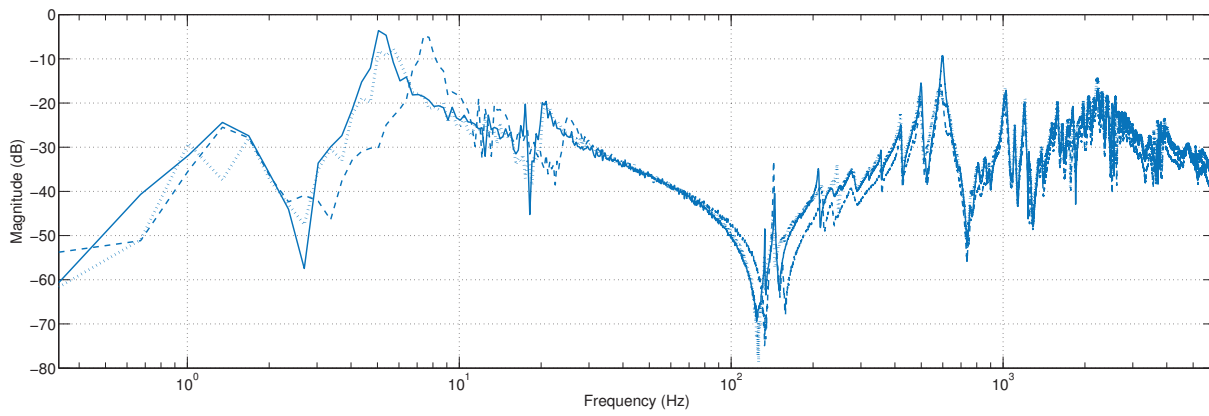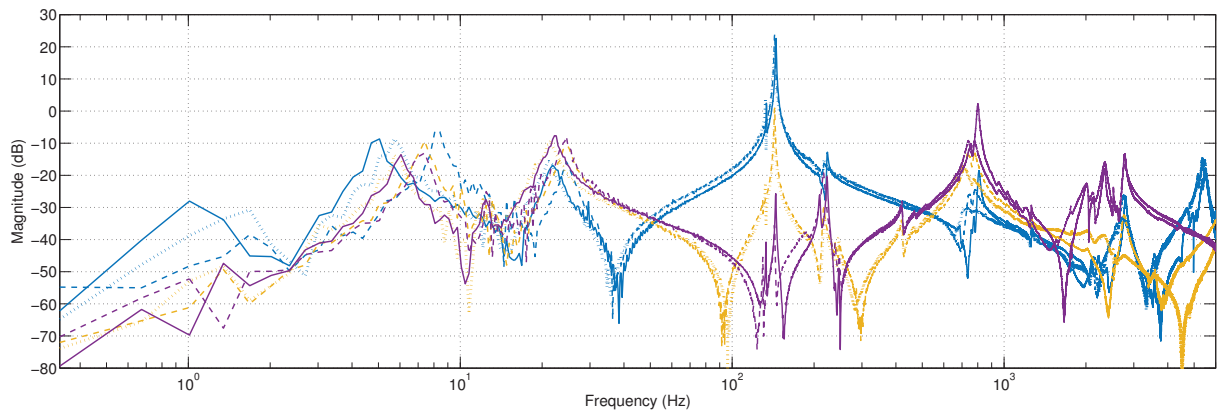
(a) (1,1)–direction
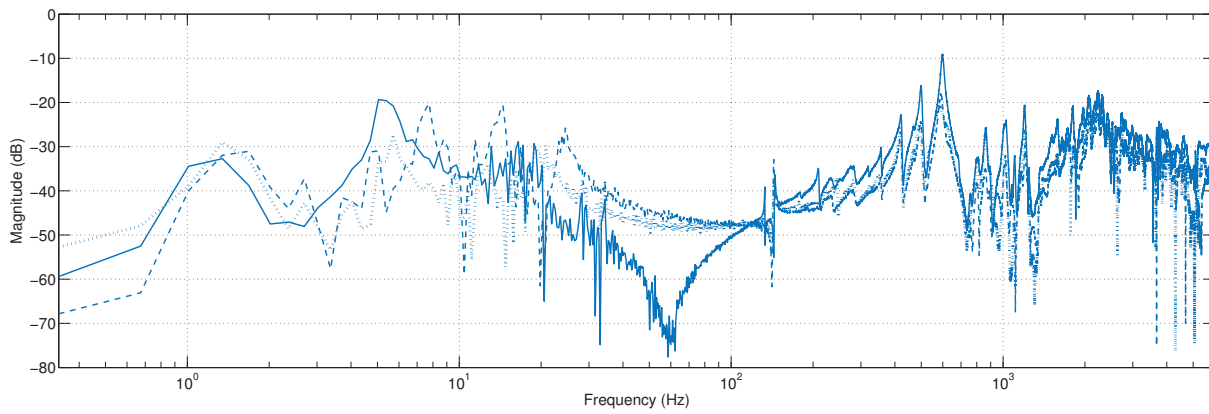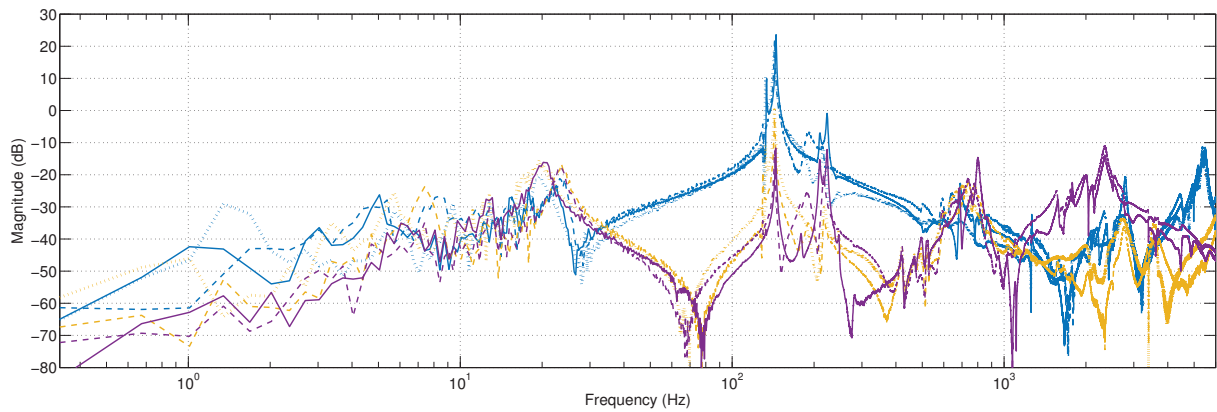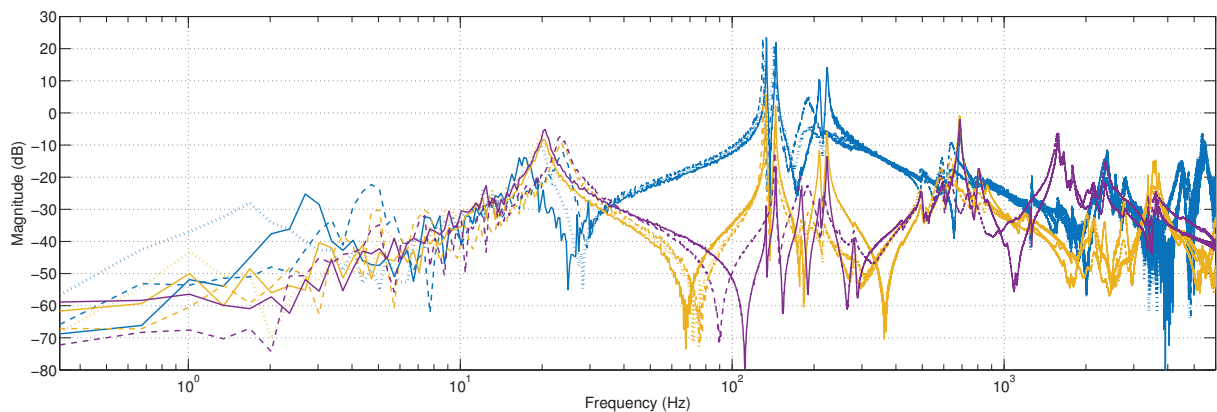

(b) (1,2)–direction

(c) (2,2)–direction

Figure 4.6: FRFs from the bridge of an unmodified violin (solid) compared with those with a 2.5 g mass attached to the tailpiece at 40 mm (dashed) and 10 mm (dotted) from the tail end.
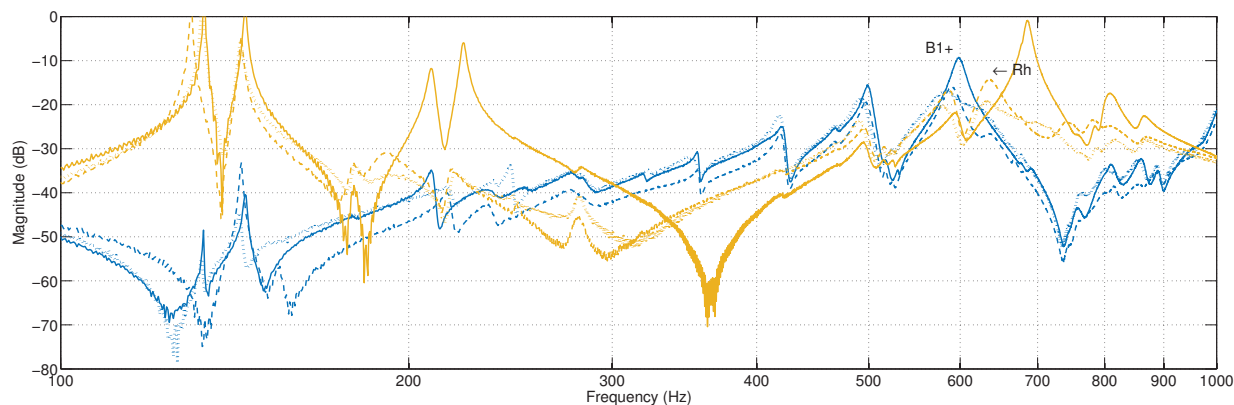
(a) (1,1)–direction

(b) (1,2)–direction

(c) (2,2)–direction

Figure 4.7: FRFs from various points along the tailpiece for the 2.5 g mass. The four impact/measurement points are indicated by the colours blue (IP 1), red (IP 2)*, gold (IP 3), and purple (IP 4), while the mass' positions are indicated by a solid line (off), dashed line (position 1), and dotted line (position 2). *Data incomplete.

Figure 4.8: FRFs from the bridge (blue) overlaid onto those from IP 2 of the tailpiece (gold) demonstrate the coupling between the B1+ and *Rh* modes after a 2.5 g mass was attached at position 1 (dashed line) and position 2 (dotted line), compared to having the mass off (solid line). The arrow indicates the downward shift of the *Rh* mode.

the solid and dashed gold lines of Figure 4.8), allowing it to absorb vibrational energy from the body much more effectively. As shown in Figure 4.8, the body's B1+ mode is much influenced by this modal interaction, and is reminiscent of the notch filtering effect observed by Stough (1996). In that study, a small 3.95 g mass attached to the tailgut end of the tailpiece (presumably near position 2) was used to lower the *Rh* mode's frequency, and the B1+ mode (referred to as the *W resonance*) fell by about 10 dB after their frequencies were matched. It remains to be seen whether lowering the rotation modes further will incite more dramatic effects; to be determined is whether the *Rh* and B1+ modes can become locked, or whether the as yet inconspicuous *Rv* mode may come to play a role.

In his custom tailpieces, White (2012) also uses a small mass of 2.5 g. The work reported here, conducted on a violin outfitted with only a "normal" tailpiece, corroborates the results reported by Pirquet (2011) and White (2012): Placing a small mass near the tail end of the tailpiece is sufficient to noticeably alter the main body modes of the violin, resulting in the lowering in frequency and amplitude of the B1+ mode. However, Pirquet and White also observed a splitting of the B1+ peak, which was not replicated to the same degree in this work. The nascent peak (in the body), induced by the *Rh* mode, is the result of the aforementioned body–tailpiece coupling, and can also be seen in Figure 4.8 (at around 630 Hz).

| Mode	Frequency (Hz)			Q			Direction 1 magnitude (dB)			Direction 2 magnitude (dB)		
A0	281	281	280	24.0	20.4	24.3	−42.9	−43.4	−39.7	−42.7	−46.2	−48.7
CBR	411	412	411	43.7	43.4	39.2	−30.2	−32.8	−32.9	−30.6	−34.4	−39.2
A1	468	467	468	52.6	53.1	52.6	−33.1	−36.3	−32.0	−38.4	−43.3	−46.3
B1−	488	488	485	50.9	46.4	48.0	−16.0	−18.6	−20.0	−25.4	−33.1	−40.4
B1+	579	568	566	33.5	21.3	14.6	−12.2	−18.7	−21.7	−17.5	−26.0	−31.3

Table 4.5: Effect of a 5.5 g mass on the signature modes. In each category, the three columns represent the measured values (from left to right) with the mass off, and with it attached at positions 1 and 2.

Even so, the degree to which the violin's perceived tone changes remains unknown. Notwithstanding the study by Wollman (2013) and the oral testimony by White, little tone quality changes could be discerned with any certainty whilst playing the instrument in a near-identical configuration. Nonetheless, the dampening of the B1+ mode signals that the wolf note has been altered – the same playing tests confirmed that the "howl" now sounded at a lower pitch. A resourceful player may find this advantageous.

4.2.2 5.5-gram mass

The second mass attached was 5.5 ± 0.25 g. The resulting bridge FRFs are shown in Figure 4.9, while the properties of the signatures modes are shown in Table 4.5. As before, the B1+ mode's frequency, quality, and magnitude were reduced while the other signature modes' were left mostly intact. But despite the heavier attachment, the direction 2 magnitude was the only value to drop more significantly than before. Nonetheless, the peak splitting is much more evident.

The complete tailpiece data set is given in Figure 4.10. Once again, the *Rh* and *Rv* modes underwent a reduction in frequency, quality, and magnitude. And as before, energy was shifted to the B1+ co-resonance (with the body) as the *Rh* mode encroaches upon it (Figure 4.11). However, the effect is noticeably more subdued this time – the rotation mode experienced a greater reduction in quality and magnitude, thus limiting its influence on the body-influenced mode. As a result, both the *Rh* and the B1+ modes appear broader – as expected of a system with increased damping. By contrast, the evolution of the *Rv* mode was more or less identical to that in the preceding experiment (2.5 g mass), leaving it still well above the signature modes.
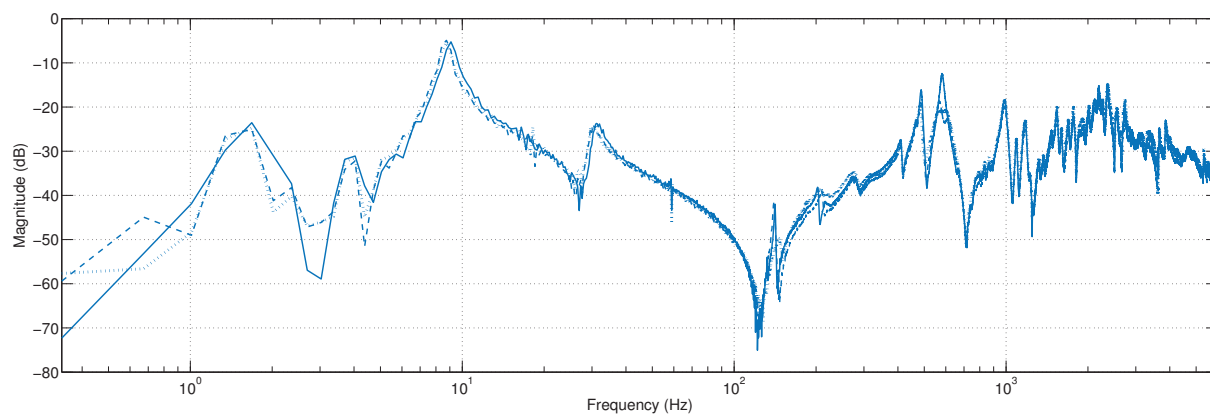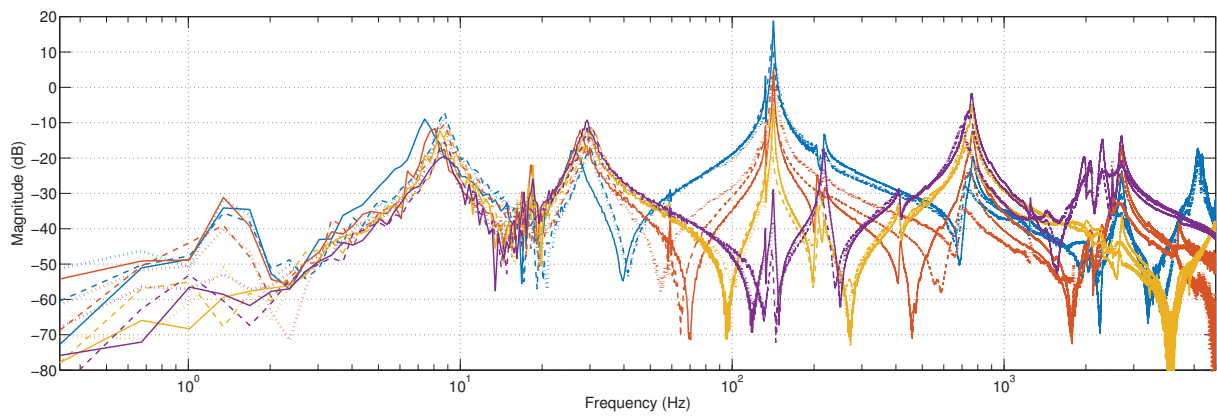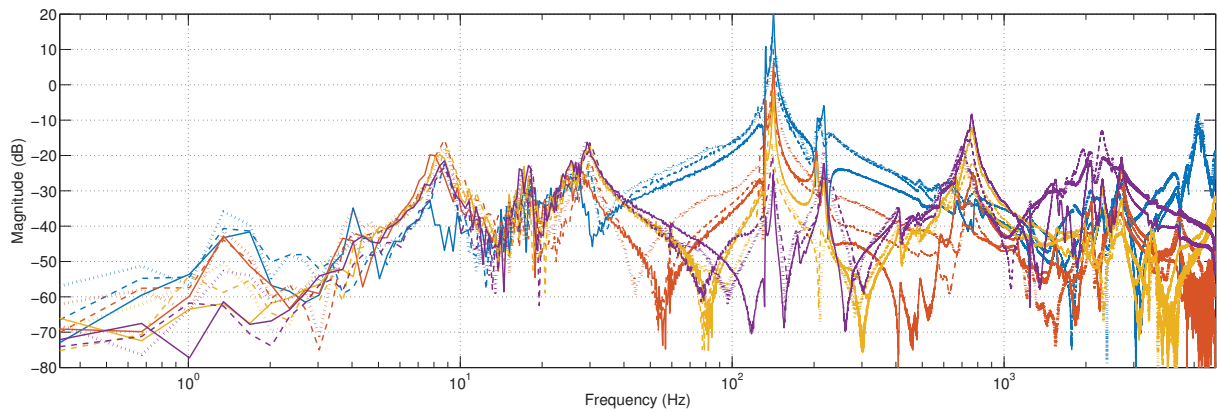
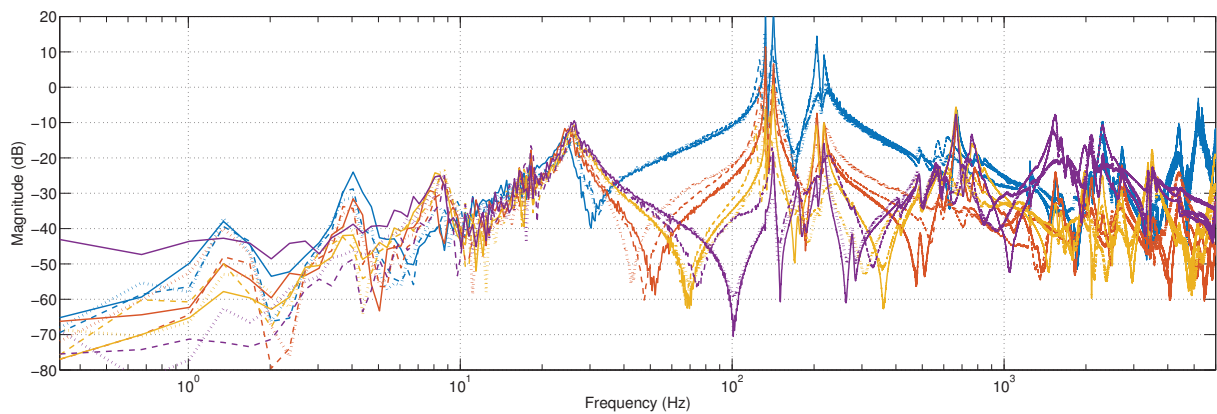(a) (1,1)–direction
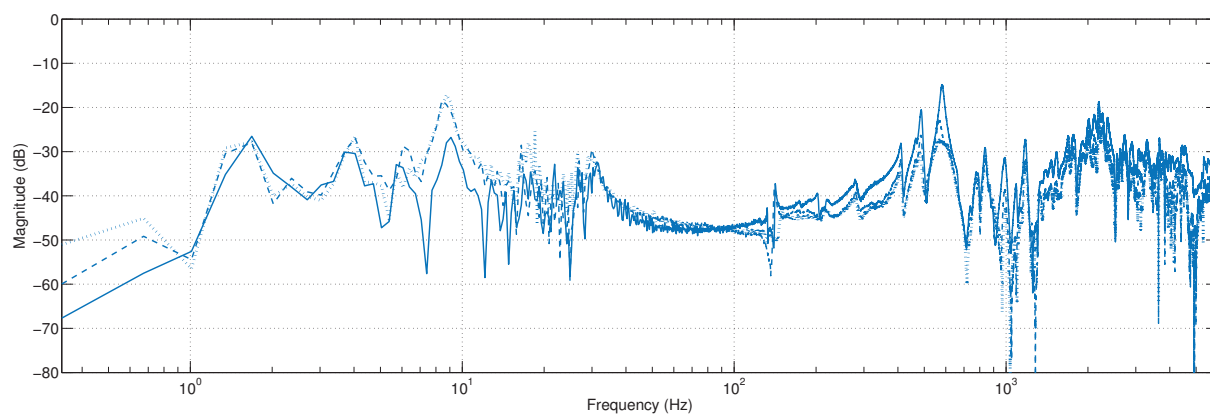
(b) (1,2)–direction
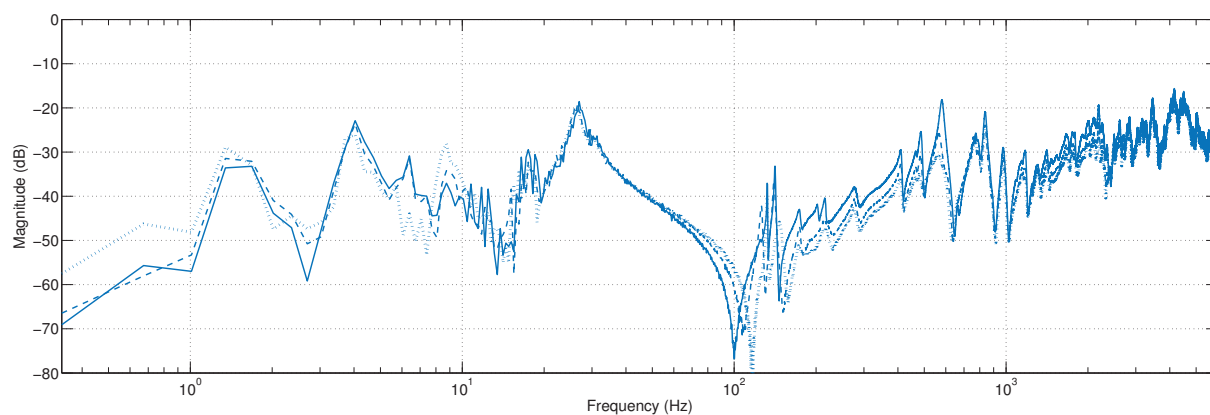
(c) (2,2)–direction

Figure 4.9: FRFs from the bridge of an unmodified violin (solid) compared with those with a 5.5 g mass attached to the tailpiece at 40 mm (dashed) and 10 mm (dotted) from the tail end.
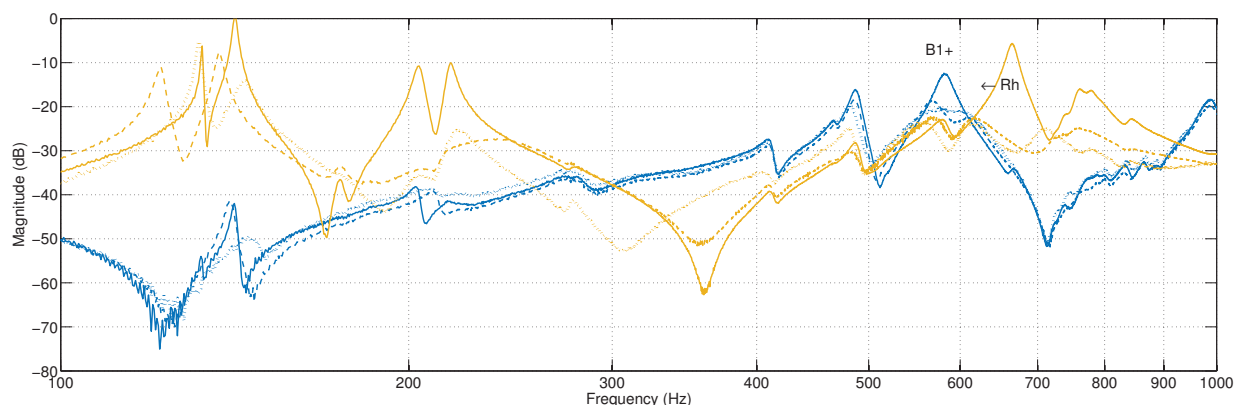
(a) (1,1)–direction

(b) (1,2)–direction

(c) (2,2)–direction

Figure 4.10: FRFs from various points along the tailpiece for the 5.5 g mass. The four impact/measurement points are indicated by the colours blue (IP 1), red (IP 2), gold (IP 3), and purple (IP 4), while the mass' positions are indicated by a solid line (off), dashed line (position 1), and dotted line (position 2).

Figure 4.11: FRFs from the bridge (blue) overlaid onto those from IP 2 of the tailpiece (gold) demonstrate the coupling between the B1+ and *Rh* modes after a 5.5 g mass was attached at position 1 (dashed line) and position 2 (dotted line), compared to having the mass off (solid line). The arrow indicates the downward shift of the *Rh* mode.

Importantly, the twin peaks around *Rh* falls neatly in line with the split B1+ peak, affirming what was previously hinted at: The rotation mode can be made to couple with the body resonances. Curiously, the *Rh*-induced peak in the bridge FRF (the higher-frequency twin of the B1+) is most prominent in direction 1 – i.e., perpendicular to the *Rh* mode itself.

Perceptually, the violin's tone became noticeably more mellow as the mass was shifted to the tail end. However, this was accompanied by an appreciable decrease in sound (volume) produced by the instrument – a not unimportant trade-off.

4.2.3 16.0-gram mass

The final mass attached was 16.0 ± 0.25 g. Against all expectations, the two breathing modes moved up in frequency even as their magnitudes dropped (Figure 4.12 and Table 4.6). Corroborating with the tailpiece data (Figure 4.13) offers little insight. The *Rh* mode at 428 Hz has fallen to irrelevance; not coinciding with any body mode, it plays no observable on role the bridge FRF. On the other hand, attaching the mass at position 1 places the *Rv* mode just above the B1+ mode, while attaching the mass at position 2 moves it to the vicinity of the B1− mode (Figure 4.14). Nonetheless, its magnitude and quality has eroded so drastically that its influence appears limited.

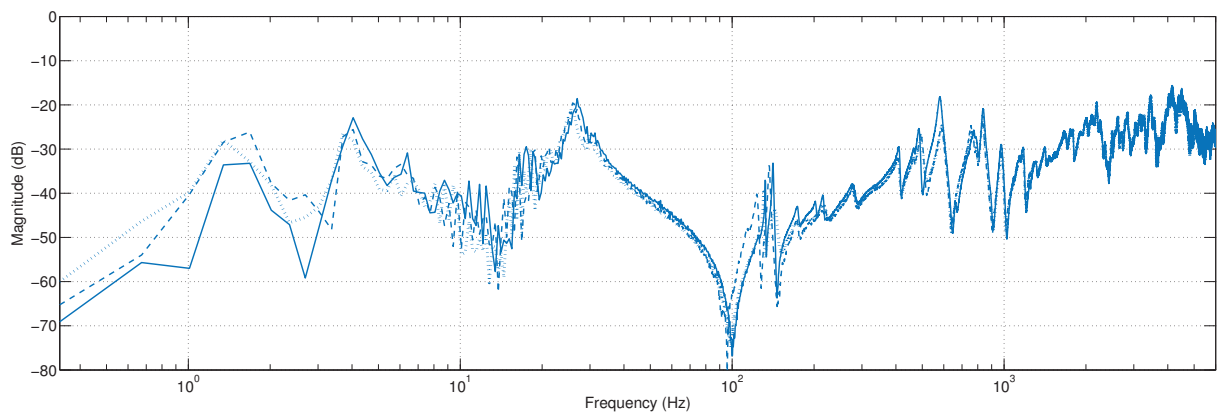Playing the instrument in this state revealed a significant deterioration in sound produced. Once again, the impact is greatest with the mass placed toward the tail end. But
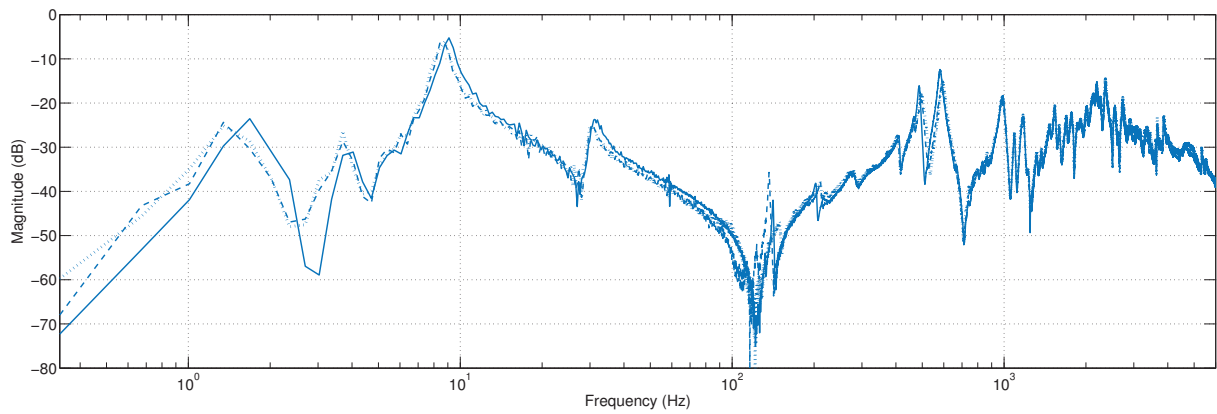
(a) (1,1)–direction
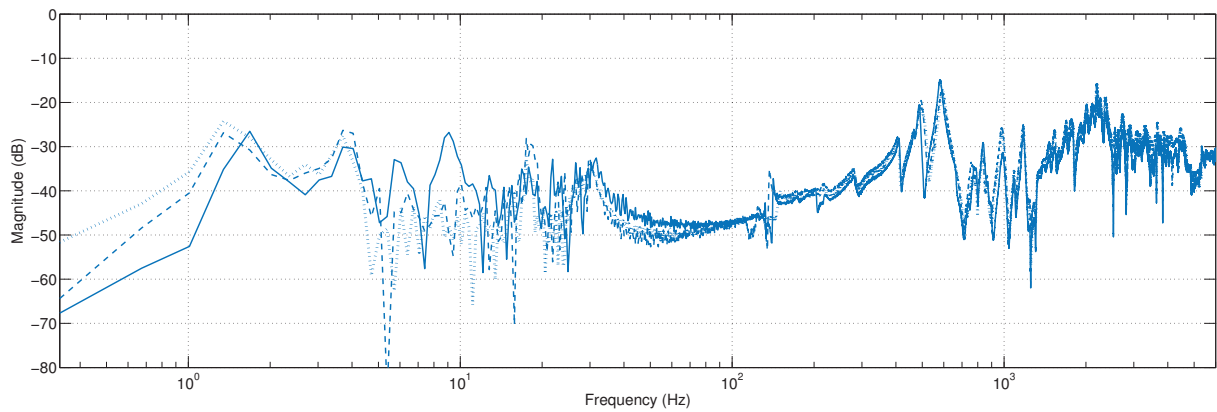
(b) (1,2)–direction

(c) (2,2)–direction

Figure 4.12: FRFs from the bridge of an unmodified violin (solid) compared with those with a 16.0 g mass attached to the tailpiece at 40 mm (dashed) and 10 mm (dotted) from the tail end.
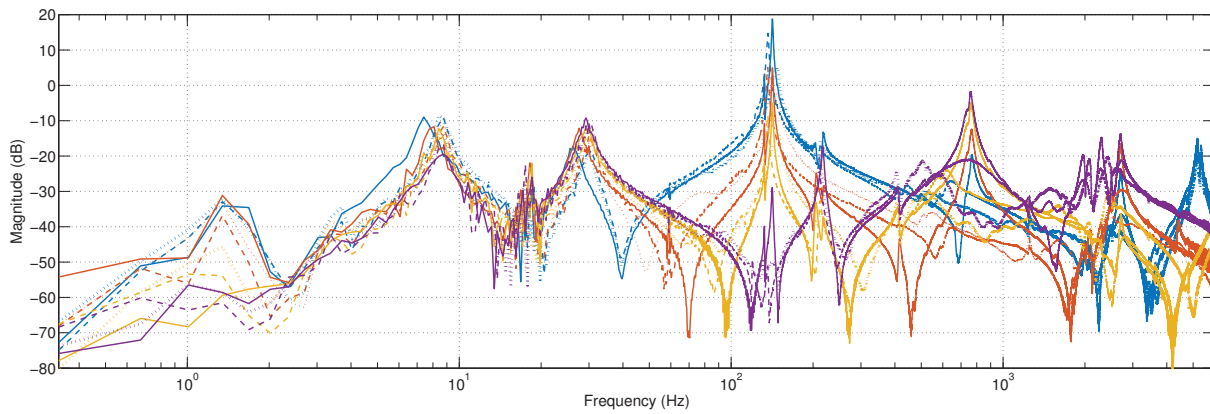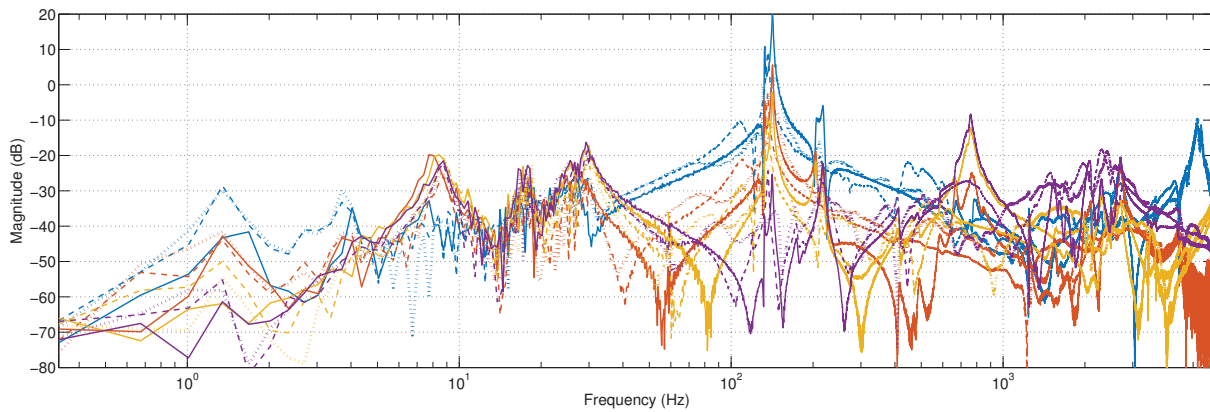
(a) (1,1)–direction
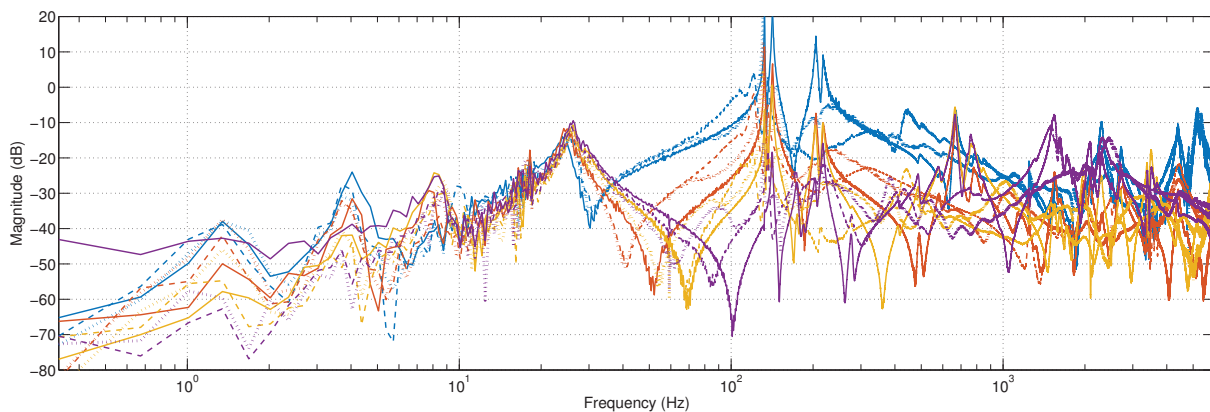
(b) (1,2)–direction

(c) (2,2)–direction

Figure 4.13: FRFs from various points along the tailpiece for the 16.0 g mass. The four impact/measurement points are indicated by the colours blue (IP 1), red (IP 2), gold (IP 3), and purple (IP 4), while the mass' positions are indicated by a solid line (off), dashed line (position 1), and dotted line (position 2).

| Mode	Frequency (Hz)			Q			Direction 1 magnitude (dB)			Direction 2 magnitude (dB)		
A0	281	281	282	24.0	44.5	19.6	-42.9	-41.2	-41.7	-42.7	-41.6	-43.9
CBR	411	408	408	43.7	37.8	31.9	-30.2	-29.4	-30.4	-30.6	-32.0	-33.0
A1	468	467	467	52.6	53.0	52.5	-33.1	-32.9	-33.4	-38.4	-39.0	-40.0
B1$-$	488	499	493	50.9	32.8	41.1	-16.0	-18.3	-19.7	-25.4	-23.8	-22.4
B1$+$	579	590	595	33.5	25.9	27.5	-12.2	-15.1	-14.6	-17.5	-21.3	-21.5

Table 4.6: Effect of a 16.0 g mass on the signature modes. In each category, the three columns represent the measured values (from left to right) with the mass off, and with it attached at positions 1 and 2.
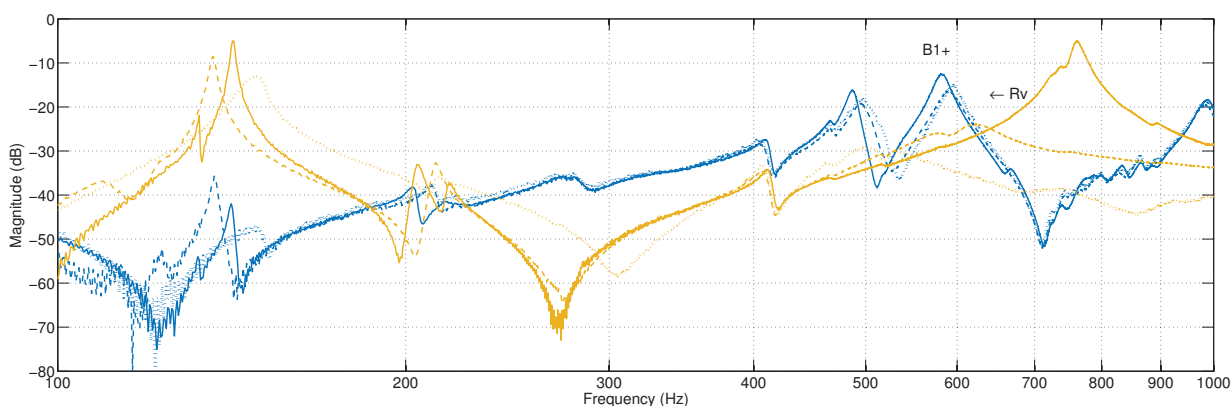
Figure 4.14: FRFs from the bridge (blue) overlaid onto those from IP 2 of the tailpiece (gold) demonstrate a possible coupling between the B1$\pm$ and *Rv* modes after a 16.0 g mass was attached at position 1 (dashed line) and position 2 (dotted line), compared to having the mass off (solid line). The arrow indicates the downward shift of the *Rv* mode.

rather differently than before, the tone does not mellow out quite as much, even as the volume decreases – as if the violin has simply been muffled. Tonally speaking, there is little to be desired in this configuration.

4.3 Fine Tuners

Finally, we turn to an issue of immediate consequence to violinists: fine tuners. A common point of contention amongst violinists and luthiers alike is whether to use a full set of fine tuners or just one for the E-string (Darnton, 1990). While fine tuners greatly ease the tuning process, especially when using metal core strings, they are comparatively

Mode	Frequency (Hz)		Q factor		Direction 1 magnitude (dB)		Direction 2 magnitude (dB)	
A0	281	282	24.0	33.5	−42.9	−39.7	−42.7	−40.8
CBR	411	411	43.7	53.4	−30.2	−28.5	−30.6	−29.5
A1	468	468	52.6	52.2	−33.1	−33.2	−38.4	−39.1
B1−	488	486	50.9	51.2	−16.0	−21.3	−25.4	−30.0
B1+	579	561	33.5	34.4	−12.2	−17.0	−17.5	−21.2
		601		28.5		−18.5		−24.8

Table 4.7: Effect of fine tuners on the signature modes. In each category, the two columns represent the measured values (from left to right) with one fine tuner attached (to the E-string) and with all four fine tuners attached.

massive – a single fine tuner weighs 5.0 ± 0.25 g. As shown previously, this amount of mass is enough to significantly alter the vibrational behaviour of the instrument. It should therefore be interesting to compare the FRFs between the two scenarios, the default setup with just one fine tuner versus the configuration with a full set. Even though the total extra mass attached is similar to the preceding trial (16.0 g), the difference is that the mass is now distributed (somewhat) evenly across the head of the tailpiece.

The resulting bridge FRFs are shown in Figure 4.15, and the tailpiece FRFs in Figure 4.16. Once again, the three lowest signature modes were largely unaffected despite the extra mass, while the B1− fell slightly in all aspects (Table 4.7). Predictably, the B1+ has split into two distinct peaks. But what is remarkable about this is the near symmetry of the two peaks, arranged about 20 Hz above and below the original peak. This may be a mere coincidence, however, as Figure 4.17 reveals that, unlike the preceding trial, the *Rh* mode has remained in the active region around 600 Hz. Indeed, it appears that the fine tuners had the most effect on the swing modes rather than the rotation modes. This is most likely due to the location of the fine tuners in relation to the node lines for these modes – this time, the extra mass is placed close to the two rotation axes while distributed away from the swing axes.

The impact on the tone, insofar as it applies to the violin at hand, is perhaps not as severe as that described by Darnton (1990). But while the violin did not sound "choked", the effect is still noticeable. Nonetheless, the increased mellowness – as well as the tamed wolf note – may be desirable on certain instruments, but the (slight) decrease in power may prove to be its Achilles heel.
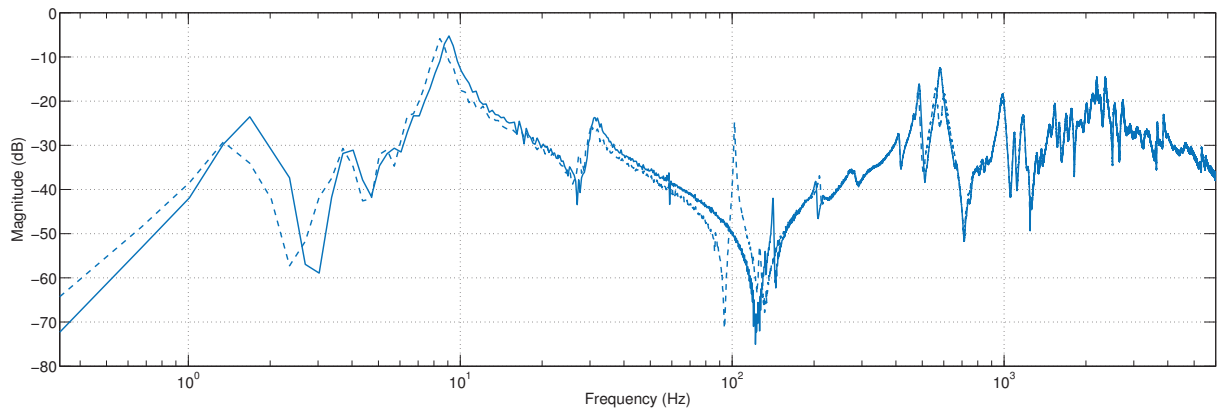
(a) (1,1)–direction
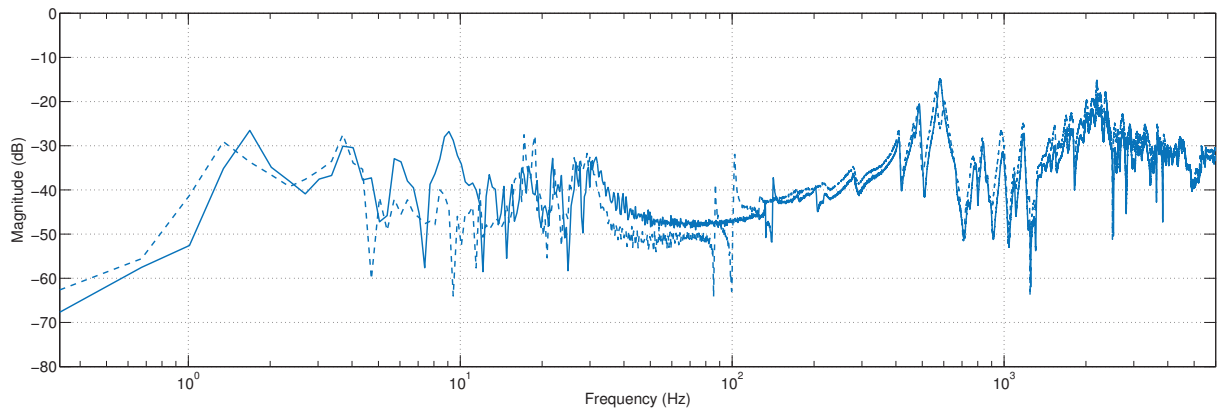
(b) (1,2)–direction
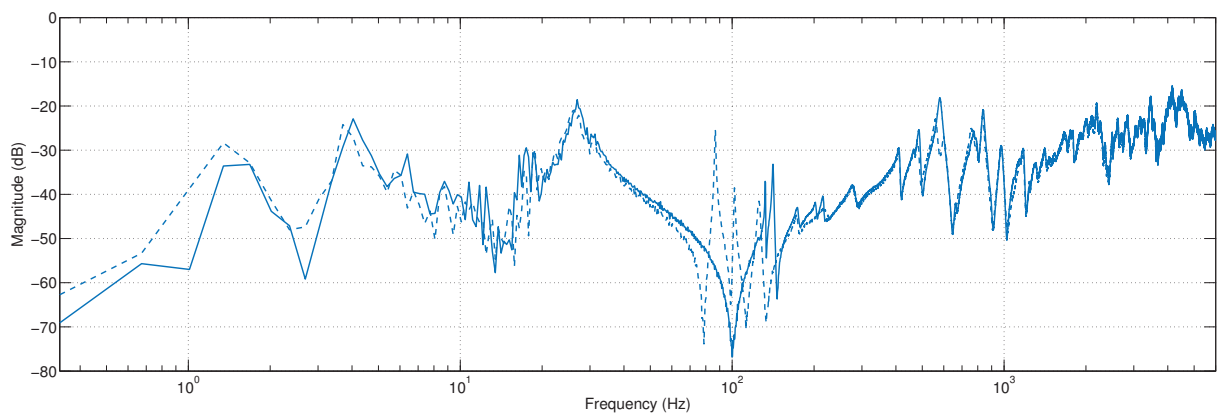
(c) (2,2)–direction

Figure 4.15: FRFs from the bridge of a violin outfitted with one fine tuner (solid) versus four (dashed).
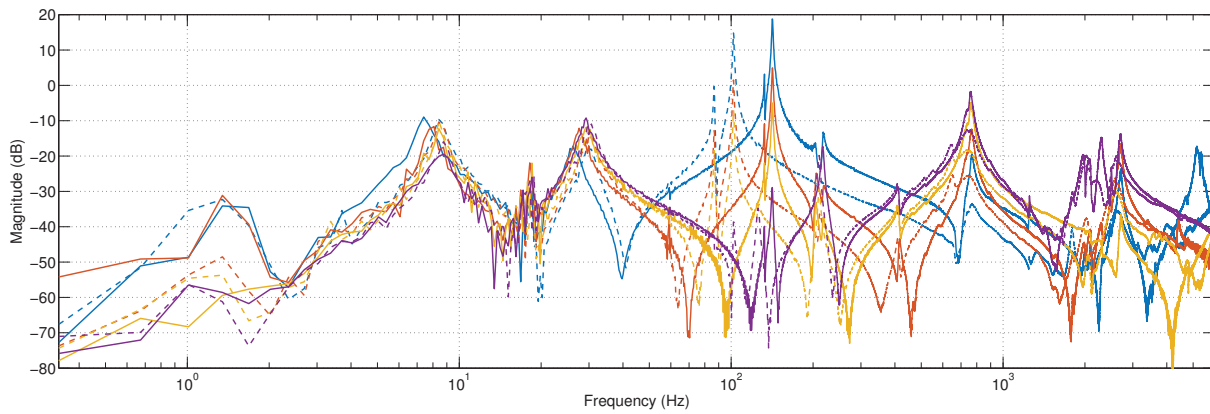
(a) (1,1)–direction
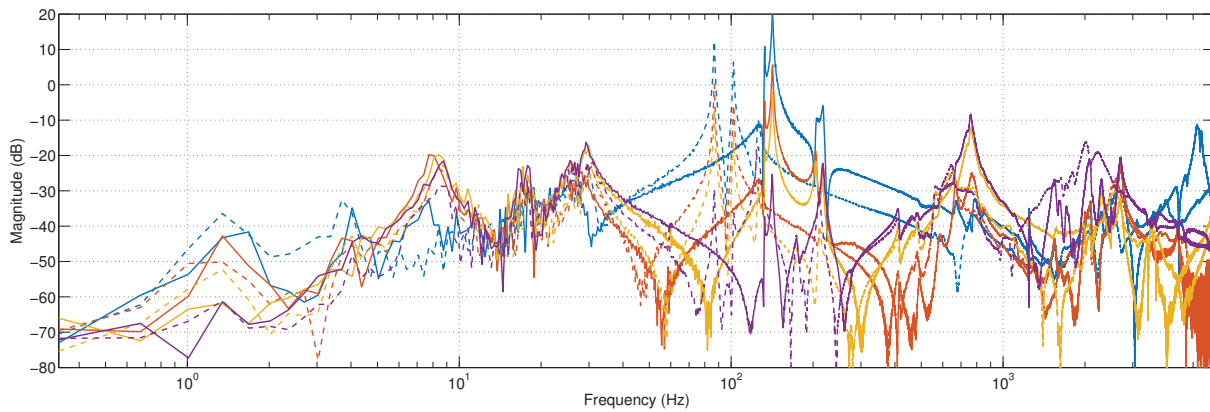
(b) (1,2)–direction
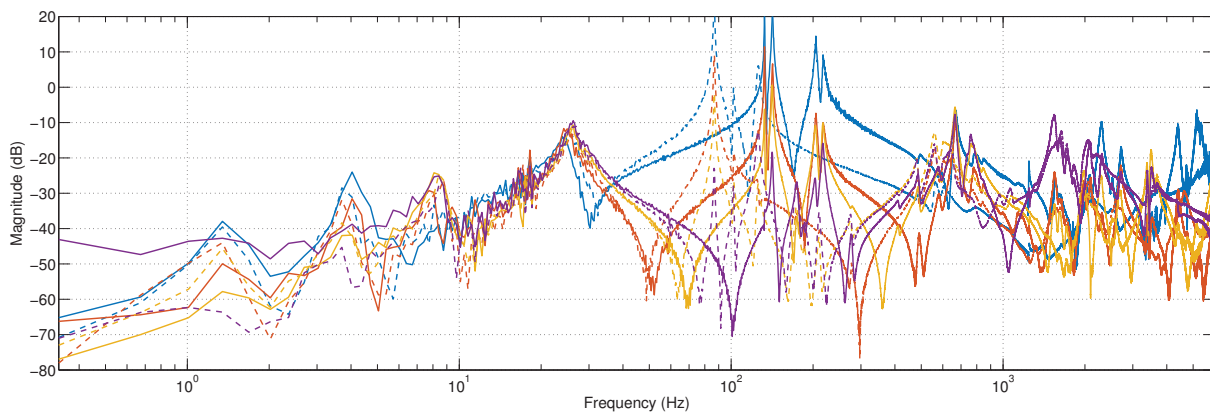
(c) (2,2)–direction

Figure 4.16: FRFs from various points along the tailpiece outfitted with fine tuners. The four impact/measurement points are indicated by the colours blue (IP 1), red (IP 2), gold (IP 3), and purple (IP 4), while the number of fine tuners deployed is indicated by a solid line (one) and a dashed line (four – a full set).

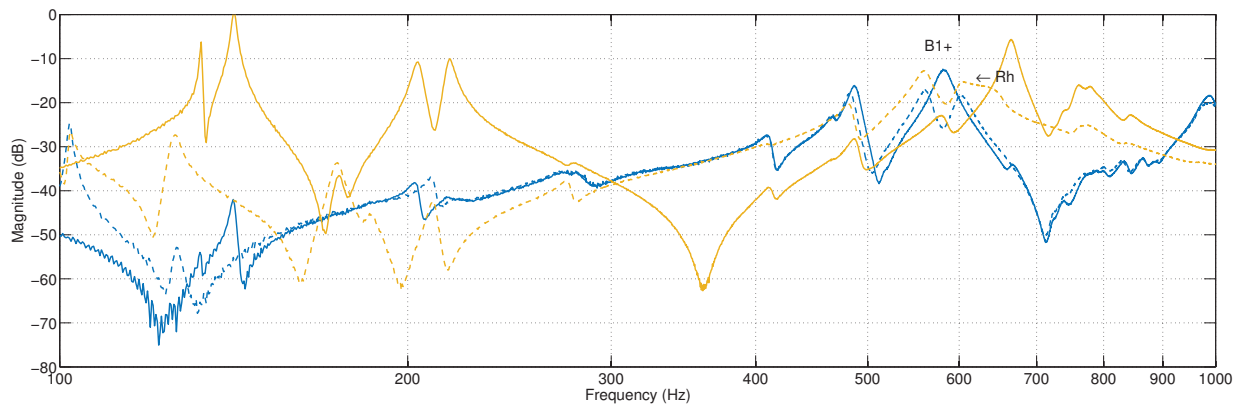**Figure 4.17**: FRFs from the bridge (blue) overlaid onto those from IP 2 of the tailpiece (gold) demonstrate the coupling between the B1+ and *Rh* modes of a violin outfitted with one fine tuner (solid) versus four (dashed). The arrow indicates the downward shift of the *Rh* mode.

4.4 Summary

Comparisons of bridge FRFs revealed that modifying the mass distribution of the tailpiece significantly altered the most prominent body vibration mode, postulated to be the B1+ mode described by Stoppani et al. (2009) and Gough (2013). Although no overall trend accounting for every scenario tested herein could be discerned, a clear correlation exists when only considering the two smaller block masses (2.5 and 5.5 $\pm$ 0.25 g). Namely, the frequency, quality factor, and magnitude of the B1+ mode were all reduced by a greater amount when using the 5.5 g mass rather than the 2.5 g mass, or when placing either of those masses at position 2 (10 mm from tail end) rather than at position 1 (40 mm from tail end). This trend did not extend to the 16 g mass, as shown in Table 4.8.

This phenomenon could be traced to the tailpiece, which exhibits two highly directional resonances lying above 600 Hz – most likely the *Rh* and *Rv* modes identified by Stough (1996). Invariably, the added mass causes a decrease in these two modes' frequencies, quality factors, and magnitudes. In the case of the 2.5 and 5.5 g masses, the *Rh* mode is able to match with the B1+ mode, resulting in a physical coupling between the tailpiece and the body that regulates their dynamical behaviour in tandem. The extra mass contributed by a full set of fine tuners can also produce a similar effect. For the 16 g mass, no such mode matching exists, though the *Rv* mode lies tantalizingly close to

Mass	Frequency	Q factor	Direction 1 magnitude	Direction 2 magnitude
2.5 g	-1.01% -1.34%	-32.8% -41.7%	-2.9 dB -3.2 dB	-5.2 dB -9.2 dB
5.0 g	-1.90% -2.25%	-36.4% -56.4%	-6.5 dB -9.5 dB	-8.5 dB -13.8 dB
16.0 g	$+1.90\%$ $+2.76\%$	-22.7% -17.9%	-2.9 dB -2.4 dB	-3.8 dB -4.0 dB
*FT	-3.11%	$+2.69\%$	-6.8 dB	-3.7 dB

Table 4.8: Relative changes to the B1+ mode effected by attaching various masses to the tailpiece. An entry with two values refers to the two positions in which the mass was attached (40 mm and 10 mm from the tail end respectively). *FT: Fine tuners (total mass: 15.0 ± 0.75 g).

the B1+ mode. Unfortunately, the *Rv* mode is too eroded to draw any conclusions; the B1+ mode's uncharacteristic rise in frequency remains unknown.

The possibility of a body–tailpiece coupling is profound. The B1+ mode is the main culprit behind the wolf note, and because it is a strongly radiating mode, it has a very noticeable effect on the tone and playability of the instrument (Stoppani et al., 2009; Gough, 2013). This study has shown that luthiers and violinists can exploit this coupling to make adjustments to tone and, as it were, "tame the wolf" by strategically changing the mass distribution of the tailpiece.

Chapter 5

Conclusions and Future Work

5.1 Conclusions

All things considered, the tailpiece appears to be a non-negligible part of the violin. Indeed, its mass distribution is a significant parameter regulating the dynamic behaviour – and hence, the tone – of the violin.

This study aims to provide a systematic account of this process and search for musically desirable configurations. To alter its moment of inertia, a series of small masses (2.5, 5.5, and 16.0 ± 0.25 g) were placed at two positions on the tailpiece (40 and 10 mm from the tail end) in succession. For each setup, two-dimensional admittance measurements at the bridge and four points along the tailpiece were acquired using a miniature impact hammer and laser Doppler vibrometer. Comparison of their FRFs revealed that the most prominent body vibration mode could be coupled with a tailpiece resonance using the two lighter masses, resulting in a lowering of its frequency, quality factor, and magnitude correlating to the weight and position of the mass. For the violinist, informal playing tests showed that this translates to a reduction of the dreaded wolf note, but also a decrease in the perceived brightness and power (loudness) of the instrument.

The experimental procedure was also repeated with the extra mass contributed by a full set of fine tuners instead of a single block mass. After extra fine tuners (5.0 ± 0.25 g each) were attached to the G-, D-, and A-string sockets, admittance measurements produced FRFs similar to the results of the 2.5 and 5.5 g masses – in spite of the fact that the total mass of the extra fine tuners (15 g) is on the order of the heaviest mass used in the previous trials (16 g).

The current work indicates that the tailpiece can be used by luthiers and violinists as an additional parameter for tone adjustment. By strategically changing its mass distribution (e.g., by attaching small masses), the tailpiece can couple with and shift the most prominent body mode, granting it the ability to change the tone colour of the instrument and to mitigate the wolf note.

5.2 Future Work

Nonetheless, it would be beneficial to determine how these results apply to different violins, which may have different setups, and to the other instruments of the violin family. During these tests, more information could be gathered about the whole tailpiece system, from bridge to tailgut. Past research has indicated that the tailgut length plays a significant role in the tailpiece's rotational modes (e.g., Stough, 1996; Fouilhé and Houssay, 2013). Unfortunately, this study was unable to address this important parameter due to physical constraints: The modern tailpiece anchors the tailgut to its reverse side, rendering it inaccessible without detaching all the strings and hence, altering the physical state of the violin. This prevents us from manipulating the mass distribution (more precisely, the rotation axes) without altering the total mass of the tailpiece, or from isolating the effects of either parameter on the vibrating modes. That said, violinists are usually unable to access the tailgut for the same reason, making mass-loading the only practical approach to exploiting the body–tailpiece coupling.

Even so, modal analysis may shed further light on the dynamic behaviour of this coupling. Presently, all characterizations of the vibrational modes are tentatively based on admittance measurements. Even though they can be good indicators of the acoustic performance of the instrument, multidimensional modal analysis – perhaps aided by numerical modeling – would provide a more definitive understanding of the body–tailpiece interactions and resolve the lingering questions from this study.

References

Ågren, C.-H., and K. A. Stetson. 1969. Measuring the wood resonances of treble viol plates by hologram interferometry. *Journal of the Acoustical Society of America* 46: 120.

Askenfelt, A. 2010. Double bass. In T. D. Rossing (Ed.), *The Science of String Instruments*, Chapter 15, 259–77. New York: Springer.

Backhaus, H. 1930. Über die Schwingungsformen von Geigenkörpern. *Zeitschrift für Physik* 62 (3–4): 143–66.

Bank, B., and M. Karjalainen. 2010. Passive admittance matrix modeling for guitar synthesis. In *Proceedings of the 13th International Conference on Digital Audio Effects (DAFx–10)*, Graz, Austria, 1–7.

Beldie, I. P. 2003. About the bridge hill mystery. *Catgut Acoustical Society Journal* 4 (8): 9–13.

Bissinger, G. 2008. Structural acoustics of good and bad violins. *Journal of the Acoustical Society of America* 124 (3): 1764–73.

Boutillon, X., G. Weinreich, and N. R. Michael. 1988. Experimental developments for the measurement of violin bridge admittance. *Journal of the Acoustical Society of America* 84: S179.

Bynum, E., and T. D. Rossing. 2010. Cello. In T. D. Rossing (Ed.), *The Science of String Instruments*, Chapter 14, 245–57. New York: Springer.

Cremer, L. 1981. *Physik der Geige*. Stuttgart: S. Hirzel Verlag. Translated by John S. Allen as *The Physics of the Violin*. (Cambridge, MA: MIT Press, 1984).

Curtin, J., and T. D. Rossing. 2010. Violin. In T. D. Rossing (Ed.), *The Science of String Instruments*, Chapter 13, 209–44. New York: Springer.

Darnton, M. 1990. Violin Setups. In T. Olsen (Ed.), *The Big Red Book of American Lutherie*, Volume 3, 352–67. Guild of American Luthiers.

Eggers, F. 1959. Untersuchung von Corpus-schwingungen am Violoncello. *Acustica* 9 (6): 463–5.

Fouilhé, E., G. Goli, A. Houssay, and G. Stoppani. 2011. Vibration modes of the cello tailpiece. *Archives of Acoustics* 36 (4): 713–26.

Fouilhé, E., and A. Houssay. 2013. String "after-length" and the cello tailpiece: Acoustics and perception. In *Proceedings of the Stockholm Music Acoustics Conference*, Royal Swedish Academy of Music, Stockholm, 60–5.

Fritz, C., I. Cross, B. C. J. Moore, and J. Woodhouse. 2007. Perceptual thresholds for detecting modifications applied to the acoustical properties of a violin. *Journal of the Acoustical Society of America* 122: 3640–50.

Fritz, C., J. Woodhouse, F. P.-H. Cheng, I. Cross, A. F. Blackwell, and B. C. J. Moore. 2010. Perceptual studies of violin body damping and vibrato. *Journal of the Acoustical Society of America* 127: 513–24.

Gough, C. 2000. Science and the Stradivarius. *Physics World* 13: 27–33.

Gough, C. 2007. Musical acoustics. In T. D. Rossing (Ed.), *Springer Handbook of Acoustics*, Chapter 15, 533–667. New York: Springer.

Gough, C. 2013. Vibrational modes of the violin family. In *Proceedings of the Stockholm Music Acoustics Conference*, Royal Swedish Academy of Music, Stockholm, 66–74.

Grant, M., and S. Boyd. 2008. Graph implementations for nonsmooth convex programs. In V. Blondel, S. Boyd, and H. Kimura (Eds.), *Recent Advances in Learning and Control*, Lecture Notes in Control and Information Sciences, 95–110. Springer-Verlag Limited. `http://stanford.edu/~boyd/graph_dcp.html`.

Grant, M., and S. Boyd. 2014. CVX: Matlab software for disciplined convex programming, version 2.1. `http://cvxr.com/cvx`. Accessed: 2015–07–20.

Gren, P., K. Tatar, J. Granström, N.-E. Molin, and E. V. Jansson. 2006. Laser vibrometry measurements of vibration and sound fields of a bowed violin. *Measurement Science and Technology* 17 (4): 635–44.

Guettler, K. 2010. Bows, strings, and bowing. In T. D. Rossing (Ed.), *The Science of String Instruments*, Chapter 15, 279–99. New York: Springer.

Helmholtz, H. v. 1863. *Die Lehre von Tonemfindungen*. Braunschweig: Friedrich Vieweg. Translated by Alexander Ellis as *On the Sensations of Tone*. (New York: Dover Publications, Inc., 1954).

Houssay, A. 2014. The string "after-length" of the cello tailpiece: History, acoustics and performance techniques. In *Proceedings of the International Symposium on Musical Acoustics*, Le Mans, France, 207–13.

Hutchins, C. M. 1981. The acoustics of violin plates. *Scientific American* 245 (4): 170–86.

Hutchins, C. M. 1983. A history of violin research. *Journal of the Acoustical Society of America* 73 (5): 1421–40.

Hutchins, C. M. 1993. The effect of relating the tailpiece frequency to that of other violin modes. *Catgut Acoustical Society Journal* 2 (3): 5–8.

Jansson, E. V. 1973. Investigation of a violin by laser speckle interferometry and acoustical measurements. *Acustica* 29 (1): 21–8.

Jansson, E. V. 1997. Admittance measurements of 25 high quality violins. *Acustica* 83: 337–41.

Jansson, E. V., I. Bork, and J. Meyer. 1986. Investigations into the acoustical properties of the violin. *Acustica* 62: 1–15.

Jansson, E. V., N.-E. Molin, and H. Sundin. 1970. Resonances of a violin studied by hologram interferometry and acoustical methods. *Physica Scripta* 2: 243–56.

Jansson, E. V., and B. K. Niewczyk. 1997. Admittance measurements of violins with high arching. *Acustica* 83: 571–4.

Jansson, E. V., and B. K. Niewczyk. 1999. On the acoustics of the violin: Bridge hill or body hill? *Catgut Acoustical Society Journal* 3 (7): 23–7.

Johannsson, H. 2015. Hans Johannsson Violins: Making. `http://hansjohannsson.com/page25/page18/making.html`. Accessed: 2015–08–01.

Lambourg, C., and A. Chaigne. 1993. Measurements and modeling of the admittance matrix at the bridge in guitars. In *Proceedings of the Stockholm Music Acoustics Conference*, Royal Swedish Academy of Music, Stockholm, 448–53.

Langhoff, A. 1994. Measurement of acoustic violin spectra and their interpretation using a 3d representation. *Acustica* 80: 505–15.

Maestre, E., G. P. Scavone, and J. O. Smith. 2013. Digital modeling of bridge driving-point admittances from measurements on violin-family instruments. In *Proceedings of the Stockholm Music Acoustics Conference*, Royal Swedish Academy of Music, Stockholm, 101–8.

McIntyre, M. E., and J. Woodhouse. 1978. The acoustics of stringed musical instruments. *Interdisciplinary Science Reviews* 3 (2): 157–73.

Meyer, J. 1972. Directivity of the bowed strings instruments and its effect on orchestral sound in concert halls. *Journal of the Acoustical Society of America* 51 (6): 1994–2009.

Nia, H. T., A. D. Jain, Y. Liu, M.-R. Alam, R. Barnas, and N. C. Makris. 2015. The evolution of air resonance power efficiency in the violin and its ancestors. *Proceedings of the Royal Society of London A* 471 (2175): 20140905.

Nolan, C. 2002. Music theory and mathematics. In T. Christensen (Ed.), *The Cambridge History of Western Music History*, Chapter 10, 272–304. Cambridge, UK: Cambridge University Press.

Pirquet, O. 2011. Violin tailpiece dynamics: Design and function. Undergraduate thesis, University of Victoria, Victoria, Canada.

Reinicke, W., and L. Cremer. 1970. Application of holographic interferometry to vibrations of the bodies of string instruments. *Journal of the Acoustical Society of America* 47: 131.

Riechers, A. 1895. *The Violin and the Art of its Construction*. Göttingen: Franz Wunder.

Rossing, T. D., F. R. Moore, and P. A. Wheeler. 2002. *Science of Sound* (3rd ed.). San Francisco: Addison-Wesley.

Saitis, C., B. L. Giordano, C. Fritz, and G. P. Scavone. 2012. Perceptual evaluation of violins: A quantitative analysis of preference judgments by experienced players. *Journal of the Acoustical Society of America* 132 (6): 4002–12.

Savart, F. 1819. Rapport sur un mémoire relatif à la construction des instruments à cordes et à archet. *Annales de chimie et de physique* 12: 225–55.

Schleske, M. 1996. Eigenmodes of vibration in the working process of the violin. *Catgut Acoustical Society Journal* 3 (1): 2–6.

Schleske, M. 2002. Empirical tools in contemporary violin making. Part II: Psychoacoustic analysis and use of acoustical tools. *Catgut Acoustical Society Journal* 4 (6): 43–61.

Stoppani, G., S. Zygmuntowicz, and G. Bissinger. 2009. Strad3D demo version: Shapes of the signature modes. `http://strad3d.org/demo/st_2.html`. Accessed: 2015–06–30.

Stough, B. 1996. The lower violin tailpiece resonances. *Catgut Acoustical Society Journal* 3 (1): 17–25.

White, T. 2012. Telling Tails. *The Strad: Accessories 2012* October: 8–12.

Willgoss, R., and R. Walker. 2007. Discernment of the sound of a violin. In *Proceedings of the 8th World Scientific and Engineering Academy and Society International Conference on Acoustics and Music: Theory and Applications*, Vancouver, Canada, 1–6.

Wollman, I. 2013. *Perception bimodale des violonistes en situation de jeu: influence des retours auditif et vibrotactile sur l'évaluation du violon*. PhD diss., Pierre and Marie Curie University, Paris, France.

Woodhouse, J. 2005. On the "bridge hill" of the violin. *Acta Acustica United with Acustica* 91: 155–65.

Woodhouse, J. 2014. The acoustics of the violin: A review. *Reports on Progress in Physics* 77 (11): 115901.

Woodhouse, J., and P. E. Courtney. 2003. The admittance matrix of a cello. In *Proceedings of the Stockholm Music Acoustics Conference*, Royal Swedish Academy of Music, Stockholm, 107–10.

Woodhouse, J., and R. S. Langley. 2012. Interpreting the input admittance of violins and guitars. *Acta Acustica United with Acustica* 98: 611–28.

Zhang, A., and J. Woodhouse. 2014. Reliability of the input admittance of bowed-string instruments measured by the hammer method. *Journal of the Acoustical Society of America* 136 (6): 3371–81.

Zygmuntowicz, S., G. Bissinger, and G. Stoppani. 2009. Strad3D demo version. `http://strad3d.org/demo/`. Accessed: 2015–06–30.